Title: Formation of subcellular compartments by condensation-prone protein OsJAZ2 in *Oryza sativa* and *Nicotiana benthamiana* leaf cells

The names of the authors:

Yoshito Koja[1#], Yu Joshima[1,2#], Yusuke Yoritaka[1], Takuya Arakawa[1], Haruka Go[1], Nagisa Hakamata[1,2], Hinako Kaseda[2], Tsukaho Hattori[1,2], Shin Takeda[1,2*]

[#]Yoshito Koja and Yu Joshima contributed equally to this work.

The affiliations of the authors:

[1]Graduate School of Bioagricultural Sciences, Nagoya University, Chikusa, Nagoya 464-8601, Japan.

[2]Bioscience and Biotechnology Center, Nagoya University, Chikusa, Nagoya 464-8601, Japan.

[*]Corresponding author (e-mail address):

Correspondence to **Shin Takeda** (takeda@agr.nagoya-u.ac.jp)

16-digit ORCID of the corresponding author:

Shin Takeda, 0000-0003-1340-8622

Abstract

Eukaryotic cells contain various membrane-less organelles, which are compartments consisting of proteinaceous condensates formed by phase separation. Such compartments are attractive for bioengineering and synthetic biology, because they can modify cellular function by the enrichment of molecules of interest and providing an orthogonal reaction system. This study reports that *Oryza sativa* JAZ2 protein (OsJAZ2) is an atypical jasmonate signalling regulator that can form large condensates in both the nucleus and cytosol of *O. sativa* cells. TIFY and Jas domains and low-complexity regions contribute to JAZ2 condensation, possibly by multivalent interaction. Fluorescence recovery after photobleaching (FRAP) analysis suggests that JAZ2 condensates form mostly gel-like or solid compartments but can also be in a liquid-like state. Deletion of the N-terminal region or the TIFY domain of JAZ2 causes an increase in the mobile fraction of JAZ2 condensates, moderately. Moreover, JAZ2 can also form liquid-like condensates when expressed in *Nicotiana benthamiana* cells. The recombinant JAZ2 fused to the green fluorescent protein (GFP) forms condensate *in vitro*, suggesting that the intermolecular interaction of JAZ2 molecules is a driving force for condensation. These results suggest the potential use of JAZ2 condensates to construct artificial membrane-less organelles in plant cells.

Keywords: Condensation-prone protein; Intrinsically disordered protein; Jasmonate; JAZ; Membrane-less organelles; Phase separation.

Key Message:

OsJAZ2 protein has a propensity to condensate, possibly by multivalent interactions, and can be used to construct artificial compartments in plant cells.

Acknowledgments

We thank Drs. M. Matsuoka and H. Yoshioka for their helpful suggestions in transient assays using rice protoplasts and *N. benthamiana*, respectively, H. Shibata and T. Kojima for useful suggestions on FRAP and SLiCE techniques, respectively, T. Nakagawa, C. Dean, and Y. Habu for the gifts of their plasmids used for the preparation of the Gateway-based vectors pUGW42 and pUGW45, the pETL8 based plasmids, carrying MBP–GFP, MBP–GFP–FCA–RRM and MBP–GFP–FCA–PrLD, and pGFP–Ex–ENS, respectively, C. Ueguchi in Nagoya University for helpful discussion, and Editage (www.editage.com) for English language editing. This work was partially supported by the Japan Society for the Promotion of Science (JSPS) KAKENHI (JP16K08140 and JP22K05427) and Nagoya University–National Institute of Advanced Industrial Science and Technology (NU-AIST) alliance project. Y. K was supported by the Japan Science and Technology Agency (JST) SPRING (JPMJSP2125) and "Graduate Program of Transformative Chem-Bio Research" in Nagoya University, supported by The Ministry of Education, Culture, Sports, Science and Technology (MEXT) (WISE Program).

Introduction

Eukaryotic cells contain membrane-less organelles consisting of proteins and other biomolecules, which are also called biomolecular condensates, coacervates, bodies, granules, paraspeckles, or droplets (Courchaine et al. 2016; Banani et al. 2017; Shin and Brangwynne 2017). Membrane-less organelles form various compartments, including nucleoli, stress granules, and processing bodies, which allow specific molecule enrichment, efficient biochemical reaction, biomolecule storage, inhibitory substance compartmentation, and protein turnover regulation (Courchaine et al. 2016; Banani et al. 2017; Shin and Brangwynne 2017; Franzmann et al. 2018; Pancsa et al. 2019). These compartments are often formed by liquid–liquid phase separation, depending on the concentration, pH, and temperature. Moreover, some condensates formed by liquid–liquid phase separation can also adopt solid or gel-like states (Kroschwald et al. 2015; Lin et al. 2015; Banani et al. 2017; Shin and Brangwynne 2017; Woodruff et al. 2017, 2018; Alberti et al. 2019; Bose et al. 2022). Membrane-less organelles will be potentially useful in bioengineering and synthetic biology because they will create platforms to modify cell function by providing an orthogonal reaction system or native protein sequestration (Reinkemeier et al. 2019; Garabedian et al. 2021; Hastings and Boeynaems 2021).

Proteins that play an important role in liquid–liquid phase separation often contain intrinsically disordered regions (IDRs), low-complexity domains (LCDs), or prion-like domains (PrLDs) (Kato et al. 2012; Hennig et al. 2015; Lin et al. 2015; Molliex et al. 2015; Patel et al. 2015; Courchaine et al. 2016; Hughes et al. 2018). Multivalent, weak non-covalent interactions between intrinsically disordered proteins (IDPs), protein–protein interactions between folded domains, and, in some cases, with other biomolecules such as nucleic acids, create a driving force for biological phase separation, condensing the proteins (Banani et al. 2017; Gomes and Shorter 2019; Alberti et al. 2019). These interactions between biomolecules include electrostatic interactions, π–cation interactions, π–π interactions, dipole–dipole interactions, hydrophobic interactions, and interactions between β-sheets

found in cross-β amyloid-like structures (Gomes and Shorter 2019; Hughes et al. 2018; Wang et al. 2018; Alberti et al. 2019; Hastings and Boeynaems 2021).

Some IDPs that undergo phase separation may form condensates *in vitro*. For instance, fused in sarcoma (FUS), a typical condensation-prone IDP comprising RNA-binding domains, LCDs, and zinc-finger domains, can condensate at 2 μM or higher concentration *in vitro*, forming not only liquid droplets, but also hydrogels or solids (Kato et al. 2012; Hennig et al. 2015; Patel et al., 2015; Courchaine et al. 2016; Wang et al. 2018). Similarly, other IDPs carrying PrLDs and RNA-binding domains, such as EWSR1, TAF15, hnRNPA1, and hnRNPA2, condensate in the micromolar range to form liquid condensates, and in some cases, hydrogels *in vitro* (Kato et al. 2012; Hennig et al. 2015; Lin et al. 2015; Molliex et al. 2015; Wang et al. 2018).

Jasmonate ZIM domain (JAZ) proteins are involved in jasmonate (JA) signalling repression in plants (Wasternack and Hause 2013; Chini et al. 2016; Huang et al. 2017; Howe et al. 2018). JA is a plant hormone that plays versatile roles in development and stress responses, particularly in defence responses (Wasternack and Hause 2013; Huang et al. 2017; Howe et al. 2018). JAZ proteins directly or indirectly repress transcription factors that activate JA-induced gene expression, such as bHLH transcription factors, including MYC2 and MYC3 of JA signalling, by recruiting a repressive complex (Toda et al. 2013; Chini et al. 2016; Huang et al. 2017; Howe et al. 2018). JA signalling is activated when plants are attacked by insects or pathogens, injured, or exposed to environmental stresses such as drought or salt damage (Wasternack and Hause 2013; Kurotani et al. 2015; Howe et al. 2018; Ogawa et al. 2021). Under these conditions, JA is synthesised and converted into jasmonoyl-Ile (JA-Ile), an active form of JA. In turn, JA-Ile binds to the COI1 receptor, a substrate recognition subunit of ubiquitin ligase, in association with the co-binding of a JAZ factor to COI1. This ubiquitinates JAZ, thereby degrading it via the 26S proteasome and de-repressing JA-induced genes (Wasternack and Hause 2013; Chini et al. 2016; Huang et al. 2017; Howe et al. 2018).

Besides these JAZ factors, atypical JAZ factors, exemplified by *Arabidopsis* JAZ7 and JAZ8 (AtJAZ7 and AtJAZ8), lack the COI1 binding site in the Jas domain, which is required for JA signalling-dependent JAZ degradation (Shyu et al. 2012). AtJAZ8 is induced by JA and involved in the negative feedback regulation of JA signalling (Shyu et al. 2012). OsJAZ2 (or OsTIFY5; Os07g0153000), *Oryza sativa* JAZ2, belongs to this class of JAZ proteins and lacks the COI1 binding site in the Jas domain (Toda et al. 2013; Hori et al. 2014). OsJAZ2 might also influence JA signalling feedback regulation, since OsJAZ2 expression levels are low under normal growth conditions but inducible by JA, based on the public expression database (RiceXpro; https://ricexpro.dna.affrc.go.jp). However, how the inhibitory effects of these atypical JAZ factors on JA-induced expression are attenuated remains unknown.

This study reports that OsJAZ2 tends to form condensates in the nucleus and cytosol when fused to the enhanced cyan fluorescent protein (eCFP) or enhanced yellow fluorescent protein (eYFP) markers, and is highly expressed in *O. sativa* and *Nicotiana benthaminana* cells transiently. OsJAZ2 condensates formed compartments resembling those formed by proteins, which caused phase separation. Moreover, OsJAZ2 often forms large condensates in *O. sativa* cytosol. Based on the characterisation of JAZ2 condensates in these plant cells, as well as *in vitro*, we discuss the possible roles of JAZ2 condensates and their potential use in constructing artificial membrane-less organelles in plants.

Materials and Methods

Plant Materials

O. sativa L. cv. 'Nipponbare' seeds were surface sterilised and germinated on a sterile 1/2 × MS medium (Murashige and Skoog basal medium, 0.35% gellan gum, pH 5.7), in a set of plant boxes (60×60×100 mm^3, CULJAR300; Iwaki, Tokyo, Japan) combined top and down. *N. benthamiana* seeds,

generous gifts from Dr. H. Yoshioka of Nagoya University, were sown on soil in plant pots. *O. sativa* and *N. benthamiana* plants were grown at 27 °C (day) and 25 °C (night) in a chamber under 16 h-light (4,500 lux) and 8 h-dark cycles. Protoplasts were isolated from the leaves of *O. sativa* seedlings harvested 6–7 days after sowing. For *Agrobacterium* infiltration, 3- to 5-week-old *N. benthamiana* leaves were used.

O. sativa protoplast isolation and transient gene expression

O. sativa leaves (upper part than the coleoptiles and lower than the lamina joint of the second leaves, except the leaf blade of the second leaves) were sliced into 0.5–1 mm pieces using a new razor blade, soaked in 0.6 M mannitol, and incubated in dark for 10 min. After removing the mannitol solution, 20 mL enzyme solution (0.6 M mannitol, 10 mM MES-KOH [pH5.7], 1.5% Cellulase R-10 [Yakult Pharmaceutical Industry, Tokyo, Japan], 0.75% Macerozyme R-10 [Yakult Pharmaceutical Industry], 0.1% bovine serum albumin [BSA], 10 mM $CaCl_2$) was added, and vacuum infiltrated into the tissues using a pump (DA-20D, ULVAC KIKO, Miyazaki, Japan), followed by incubating in dark for 5 h with gentle agitation (75 rpm) at 25 °C. After enzymatic digestion of the cell walls, 20 mL W5 solution (154 mM NaCl, 125 mM $CaCl_2$, 5 mM KCl, 2 mM MES-KOH [pH5.7]) was mixed, filtered through an autoclaved polyester mesh cloth (PET73), and centrifuged at 500× *g* for 2 min. The precipitates were suspended in 2 mL W5 solution, filtered, and re-centrifuged. The supernatants were filtered and centrifuged similarly once or twice. Finally, all precipitates were suspended in 2 mL W5 solution and re-centrifuged. The final precipitate was suspended in 0.5–2 mL MMg solution (0.4 M mannitol, 15 mM $MgCl_2$, 4 mM MES-KOH [pH5.7]). Isolated protoplasts in the solution were counted using a haemocytometer under a microscope and diluted with the same buffer solution to a cell density of 2×10^6–2×10^7 cells/mL.

Then, 10–20 μL DNA solution containing plasmids of interest (5 μg for each plasmid in

normal experiments, unless otherwise mentioned) was mixed with 100 μL protoplast suspension solution and equal volume (to DNA and protoplast solution) PEG solution (40% PEG4000 [SIGMA 81420, Merck KGaA, Darmstadt, Germany], 0.2 M mannitol, 0.1 M $CaCl_2$) in a round-bottomed microcentrifuge tube. After incubation approximately at 25 °C for 10–20 min, W5 solution (four times PEG solution volume) was added, mixed gently, and then centrifuged at 500× *g* for 2 min. The precipitates were suspended in 300 μL WI solution (0.5 M mannitol, 4 mM MES-KOH [pH5.7], 20 mM KCl). The protoplasts were incubated at 22 °C in dark for 16–22 h in a horizontally fixed tube. Under nutrient-rich conditions, protoplasts were incubated in R2P liquid medium containing 2 mg/L 2,4-D and 13.7% sucrose (Ohira et al. 1973). For microscopic observation, 23 μL protoplast solution was placed on an MAS-coated glass slide (SMAS-01, Matsunami Glass Ind., Osaka, JAPAN) with a spacer (Secure-Seal Imaging Spacers, 20 mm diameter × 0.12 mm depth, GRACE BIO-LABS, Bend, OR, USA) attached and overlaid with a coverslip (22×22 mm^2, Matsunami Glass Ind.). For osmotic protoplast burst, equal H_2O volume was added to the protoplast solution and immediately used for time-lapse imaging.

For treatment of protoplasts with 1,6-hexanediol (HD; #081-00435, WAKO, Japan), 50% 1,6-HD dissolved in WI solution was added to the protoplast solutions to final concentrations of 5% and 10%. After incubation approximately at 25 °C for 5–30 min, protoplast solutions were placed on MAS-coated glass slides.

Agrobacterium **infiltration of** ***N. benthamiana***

Agrobacterium infiltration of *N. benthamiana* using pSoup- and pGeenII-derived plasmids was performed as previously described (Hellens et al. 2000; Asai et al. 2008). The plasmids were introduced into *Agrobacterium tumefaciens* (strain GV3101) by electroporation. The transformed *Agrobacterium* cell cultures were infiltrated into *N. benthamiana* leaves and incubated in the plant

chamber for 2–3 days. For microscopic observation, leaf segments (1×2 cm^2) were mounted upside-down on glass slides (S2441, Matsunami Glass Ind.,) with coverslips and sterile water.

Microscopic observation and fluorescence recovery after photobleaching (FRAP) analysis

The fluorescence of reporter proteins was observed under a confocal laser scanning microscope (CLSM; FV 1000, Olympus, Tokyo, Japan) at 440/460–500, 515/530–545 nm, and 559/575–675 nm (excitation/emission wavelengths) for CFP, YFP, and red fluorescent protein (RFP), respectively. Green fluorescent protein (GFP) fluorescence of the recombinant proteins was observed using CLSM at 473 or 488 nm (excitation wavelengths) and 491–535 nm (emission wavelengths). For observing *O. sativa* cells, monomeric RFP1 (mRFP1) -expressing protoplasts were selected by introducing the pDH51–mRFP1 plasmid carrying the CaMV35S promoter-driven *mRFP1* gene. To visualise the nucleus, a pUGW42-based plasmid carrying the CaMV35S promoter-driven *eYFP–OsbHLH094* gene (*Os07g0193800;* Toda et al. 2013) was introduced into *O. sativa* protoplasts. For control experiments with *O. sativa* cells expressing eCFP alone, pUGW45 was used. To distinguish the localisation of condensates inside and outside of the nucleus, observation was carried out by shifting the focal plane. We used a 20× objective lens for normal observation, a 60× objective lens for FRAP analysis, and an 100× objective lens for observation as in **Fig. 1C** and **Supplementary Fig. 3**. For FRAP analysis of condensates formed *in vivo*, circular areas (radius: 0.8–1 μm for *O. sativa* and 1.6 μm for *N. benthamiana*) were bleached for 0.5 s, using tornado bleach pulse, and CFP fluorescence recovery was monitored continuously without interval setting. For FRAP analysis of GFP–JAZ2 condensates formed *in vitro*, GFP foci were photo-bleached with a 488 nm laser pulse (3 frames, 25%), and GFP fluorescence recovery was monitored at 1 s intervals for 4 min. Fluorescence intensity of the region of interest (ROI) was measured using FV1000 software or FIJI/ImageJ. Normalised fluorescence intensity (I_{nor}) was calculated as follows;

$$Inor = \frac{It - BGt}{Ipre - BGave}$$

where I_t and BG_t are the fluorescence intensity and background at time point t, and I_{pre} and BG_{ave} are the average intensity and background of 50 frames before bleaching, respectively.

Plasmid construction

The plasmids used for CaMV 35S promoter-mediated eYFP- and eCFP-fused JAZ2 expression in *O. sativa* protoplasts, pUGW42_eYFP–JAZ2 and pUGW45_eCFP–JAZ2, respectively, were prepared as follows. cDNA encoding OsJAZ2 (Toda et al. 2013), sub-cloned into pENTR-/D-Topo (Invitrogen, Thermo Fisher Scientific K.K., Tokyo, Japan)(Hori et al. 2014), was inserted by LR reaction into a gateway-based vector pUGW42 or pUGW45. To express the eCFP–JAZ2 variants carrying various deletions or amino acid substitutions, site-directed mutagenesis was performed by PCR amplification of pUGW45_eCFP-JAZ2 with the mutated primer sets (**Supplementary Table 1**) and KOD FX-Neo DNA polymerase (TOYOBO, Osaka, Japan), followed by *Dpn*I digestion and transformation into *E. coli* DH5-α or XL1-Blue. For eCFP-fused JAZ9 (Os03g0180800) construction, *OsJAZ9* cDNA (Toda et al. 2013) was amplified by PCR using forward and reverse primers containing *Not*I and *Mlu*I sites (**Supplementary Table 1**), respectively. The amplified DNA was digested with *Not*I and *Mlu*I and inserted between *Not*I and *Asc*I sites of pUGW45_eCFP–JAZ2, instead of JAZ2, thus forming pUGW45_eCFP–JAZ9. pUGW42-based plasmids for eYFP–TIFY–LCR2 and eYFP–LCR5–Jas were prepared using SLiCE (Motohashi 2015), a seamless cloning method, with the indicated primer sets (**Supplementary Table 1**).

The plasmids used for *Agrobacterium* infiltration of *N. benthamiana* were constructed as follows. A DNA segment containing *2x CaMV 35S* enhancer, basal promoter, TEV leader sequence (tobacco etch virus 5′-leader sequence, *TL*; Niepel and Gallie, 1999), and *eGFP* reporter was prepared by *Hin*dIII digestion of pGFP–Ex–ENS and inserted into *Hin*dIII site of pGreen II (Hellens et al. 2000),

resulting in pGreen II–*2x* 35S-TL–eGFP. *eGFP* of pGreen II–*2x* 35S-TL–eGFP was substituted with *eCFP*, *eYFP*, *eCFP–JAZ2*, and *SCAMP1*$^{\Delta N118}$*-eYFP* using the SLiCE method (Motohashi 2015), using primer sets as indicated (**Supplementary Table 1**). A cDNA fragment of *OsSCAMP1* (XM_015789328) encoding SCAMP1$^{\Delta N118}$, OsSCAMP1 that lacks 118 N-terminal amino acids, was prepared by PCR amplification from an *O. sativa* basal shoot region-derived cDNA mixture using specific primer sets (**Supplementary Table 1**) and PrimeSTAR GXL DNA polymerase (Takara Bio, Shiga, Japan).

A plasmid used for recombinant Maltose-binding protein (MBP)–GFP–JAZ2 protein expression was constructed by inserting cDNA encoding OsJAZ2 into pETL8–GFP, a pET11 (Novagen, Merck KGaA)-based plasmid, carrying MBP-fused GFP (Fang et al. 2019). JAZ2 cDNA was amplified by PCR with the primer set indicated in **Supplementary Table 1** using KOD FX-Neo DNA polymerase (TOYOBO), digested with *Bsp*HI and *Sal*I, and inserted between the *Nco*I and *Xho*I sites of pETL8–GFP, forming pETL8_GFP–JAZ2.

Recombinant protein expression and purification in *E. coli* and *in vitro* condensation

MBP-fused proteins were expressed in *E. coli* strain BL21 (DE3). *E. coli* cells were cultured in a liquid medium (rich broth supplemented with glucose) at 37 °C with shaking at 105 rpm until the culture absorbance at 600 nm reached 0.4–0.5. The cells were cooled on ice and cultured in the presence of 0.5 mM isopropyl ß-D-1-thiogalactopyranoside (IPTG) at 18 °C with shaking overnight.

MBP-fused proteins were purified using amylose-resin (E8021S, New England Biolabs Japan Inc., Tokyo, Japan). The cells were harvested by centrifugation at 4,000× *g* at 4 °C for 10 min, resuspended in 5 mL column buffer (20 mM Tris-HCl [pH 7.4], 200 mM NaCl, 1 mM EDTA [pH 8.0], cOmplete, EDTA-free [Roche, Merck KGaA], 1 mM dithiothreitol [DTT]), frozen at −20 °C, thawed in a water bath at 37 °C until only a few ice pieces remained, and the remaining ice pieces were thawed

by gentle tumbling and mixing. The cells were sonicated in an ice-cold water bath in 10 cycles of 10 s bursts with 60 s cooling intervals using a sonicator (BRANSON SONIFIER 450, Branson Ultrasonics Corp, CT, USA) at output control 3 and 30% duty cycle. The cell lysate was centrifuged at 9,000× *g* for 20 min at 4 °C and separated into soluble and insoluble fractions. The soluble fractions were aliquoted into several microtubes, frozen in liquid nitrogen, and stored at −80 °C.

The soluble fraction (70–140 μL) was incubated with 30–35 μL (bed volume) pre-washed amylose-resin in a 1.5 mL tube for 2 h at room temperature, with gentle agitation using a seesaw shaker (BC-700, BIO CRAFT, Tokyo, Japan). The resin-bound MBP-fused protein was collected by centrifugation at 3,300× *g* for 1 min. After removing the supernatant, the MBP-fused protein was washed with 1 mL column buffer, collected by centrifugation, eluted by incubation with 80 μL column buffer supplemented with 10 mM maltose for 10 min at room temperature with gentle agitation, recovered in the supernatant by centrifugation at 3,300× *g* for 1 min, and stored at 4 °C. The MBP-tag was separated from the protein of interest by cleavage with TEV protease (12575-015, Invitrogen) at 30 °C for 2 h after adding an equal volume of 2× TEV cleavage buffer (100 mM Tris-HCl pH 8.0, 1 mM EDTA) and 1 mM DTT final concentration. NaCl concentration in the buffer for cleavage by the TEV protease was increased to examine condensation in the presence of increased NaCl concentration. IPTG induction, purification using amylose-resin, and MBP-tag cleavage of proteins were confirmed by SDS−PAGE analysis. The amount of protein after MBP-tag cleavage was estimated from the staining of bands on SDS−PAGE with BSA as a standard. For microscopic observation, 8 μL protein solution was placed on a glass slide (S024410, Matsunami Glass Ind.) and overlaid with a coverslip. The protein samples were incubated at 23–25 °C for 19 h after the TEV protease reaction at 30 °C for 2 h for observing long time-dependent condensate formation.

For treatment of GFP–JAZ2 condensates with 1,6-HD, 50% 1,6-HD dissolved in H_2O, together with the TEV protease reaction buffer premix containing the column buffer, was added to the

protein solution after the TEV protease reaction to a final concentration of 10% 1,6-HD. The protein solution was then placed on a glass bottom dish (D141400, Matsunami Glass Ind.) and immediately used for observation of GFP at 488/500–515 (excitation/emission wavelengths) under a CLSM (FV 3000, Olympus, Tokyo, Japan) with a 60x objective lens.

Results

eCFP–JAZ2 expression causes condensate formation in *O. sativa* protoplasts

Subcellular localisation of several JAZ factors and other nuclear proteins in *O. sativa* indicated that eCFP-fused OsJAZ2 (eCFP–JAZ2) frequently formed condensates when transiently expressed in *O. sativa* protoplasts (**Fig. 1**). The CFP fluorescence of eCFP–JAZ2 was detected in not only the nucleus, but also the cytosol with strong foci. JAZ2 condensates in the cytosol were frequently observed in the vicinity of the nucleus (**Fig. 1, Supplementary Fig. 1**), possibly reflecting the cytosolic condensation-dependent nuclear localisation inhibition. Extensive observations showed that eCFP–JAZ2 also formed condensates in the nucleus (**Fig. 1C**). Such foci were scarcely observed with other nuclear factors, such as for eCFP-fused JAZ9 (or OsTIFY11a) (**Supplementary Fig. 2**), a typical JAZ protein that can bind to COI1 and is degraded in a JA signalling-dependent manner (Toda et al. 2013; Wu et al. 2015), and for eYFP-fused bHLH094 that was used for nucleus visualisation in this study (Toda et al. 2013) (**Fig. 1, Supplementary Figs. 1, 2**). In both cases, eCFP and eYFP signals were detected predominantly in the nucleus (**Fig. 1, Supplementary Figs. 1, 2**). CFP fluorescence of eCFP–JAZ9 was weaker than that of eCFP–JAZ2 in most cells, probably due to JAZ9 degradation. JAZ2 condensates were detected in 45–100% of the observed cells, depending on the experiments (mean ± s.d., 86±16%, n=20). Notably, eCFP–JAZ2 occasionally forms extremely large condensates in the cytosol, which is nearly comparable to the nucleus in size (**Fig. 1, Supplementary Fig. 1**). Moreover, signals of the fluorescent protein, mRFP1, another marker protein used for both nucleus and cytosol

visualisation, were often less visible at the site of eCFP–JAZ2 condensates (**Fig. 1, Supplementary Figs. 1, 3**). This implies that eCFP–JAZ2 condensates form subcellular compartments. eYFP–bHLH094 was occasionally excluded from JAZ2 condensates, but sometimes combined with JAZ2 condensates.

eCFP–JAZ2 forms stable condensates in *O. sativa*

The eCFP–JAZ2 condensates observed in *O. sativa* cells varied in size and shape; condensates observed in the nucleus were relatively small and spherical or ellipsoidal (0.5–1.5 μm diameter), whereas those in the cytosol were often large and non-spherical or non-ellipsoidal (up to approximately 7 μm diameter; **Fig. 1, Supplementary Figs. 1, 3**). In some cases, eCFP–JAZ2 condensates in the nucleus and cytosol appeared to form a connection, possibly through the nuclear pores (**Supplementary Fig. 3**). Protoplast burst by changing osmotic pressure immediately diffused cytosolic mRFP1, but not eCFP–JAZ2, signals in the vicinity of the nucleus (**Supplementary Fig. 4A**). Treatment of protoplasts with 1,6-hexanediol, which is widely used to distinguish between liquid and solid condensates (Kroschwald,et al. 2017; Alberti et al. 2019), had little effect on eCFP–JAZ2 condensates (**Supplementary Fig. 4B**). These observations suggest that eCFP–JAZ2 forms stable condensates.

In this study, protoplasts were incubated in a nutrient-poor solution after plasmid DNA introduction. Thus, whether cell starvation might cause eCFP–JAZ2 condensate formation, similar to yeast starvation-induced proteasome storage granule, solid-like Cdc19 aggregate, or Sup35 condensate formation (Laporte et al. 2008; Saad et al 2017; Franzmann et al. 2018), should be studied. However, eCFP–JAZ2 condensed even when protoplasts were incubated in a nutrient-rich R2P medium (**Supplementary Fig. 5A**).

When eCFP alone was expressed, CFP foci reflecting protein condensation were not

detected (**Supplementary Fig. 5B**). Since GFP-derived proteins, such as CFP, can form dimers, we examined JAZ2 fusion to eCFP^{A207K}, which carries a mutation to avoid dimerisation of GFP derivative makers (Zacharias et al. 2002; Segami et al. 2014). eCFP^{A207K}–JAZ2 developed CFP foci, indicating condensation, although the condensate formation frequency depended on the presence or absence of YFP–bHLH094 (**Supplementary Fig. 5C**). JAZ2-fused eYFP also produced eYFP foci (**Supplementary Fig. 5D**), indicating that JAZ2-mediated foci are not necessarily linked to CFP fluorescence. Taken together, these results suggest that JAZ2 is a condensation-prone protein. This was further confirmed by mutational analyses of JAZ2 and *in vitro* condensation experiments, as described below.

JAZ2 low-complexity regions are involved in condensate formation

OsJAZ2 has IDRs with five low-complexity regions (LCRs), in addition to an EAR motif and the TIFY and Jas domains, which are highly conserved among JAZ factors (**Fig. 1A**), whereas OsJAZ9 possesses only two LCRs (**Supplementary Fig. 2**). Moreover, the existence of a PrLD was predicted in OsJAZ2 at the second LCR (LCR2) (**Fig. 1A**), but not OsJAZ9 (**Supplementary Fig. 2**). Deletions of regions containing LCR1, LCR2, or LCR3 and LCR4 decreased eCFP–JAZ2 condensate formation frequency, although the extent of their effects varied between experiments (**Supplementary Fig. 6**). Deletion of a region containing LCR3–LCR5 resulted in a more drastic decrease in condensation frequency (**Supplementary Fig. 6**). These results suggest that LCRs are involved in eCFP–JAZ2 condensation. It should be noted that LCR3–LCR4 deletion weakened the overall CFP signals, and finding cells with sufficient CFP signals for observation was relatively difficult.

TIFY and Jas domains contribute to JAZ2 condensate formation

Next, whether the conserved domains among JAZ factors are involved in JAZ2 condensate formation

were examined because they contain amino acid sequences predicted to generate amyloid-like structures using the FoldAmyloid program (Garbuzynskiy et al. 2010) (**Fig. 2A**). The TIFY domain contains two β-strands forming an antiparallel β-sheet (**Fig. 2B**), raising the question whether these cause weak interactions between the molecules. EAR motif and TIFY and Jas domain deletions revealed that the Jas domain was required for eCFP–JAZ2 condensation, in addition to its function in nuclear localisation (Withers et al. 2012) (**Fig. 3 and Supplementary Fig. 7**). The TIFY domain positively affected JAZ2 condensate formation, whereas the contribution of the N-terminal region containing the EAR motif differed depending on the experiment (**Fig. 3 and Supplementary Fig. 7**). Additional deletion analysis showed that not only the N-terminal part containing the two β-strands, but also the C-terminal part of the TIFY domain could be involved in JAZ2 condensate formation and most amino acids forming the two β-strands, including two aromatic residues (Phe and Tyr), were not necessary for JAZ2 condensation (**Supplementary Fig. 8**).

The Jas domain of JAZ2 is rich in basic amino acids, such as Lys and Arg (K, R; **Fig. 2, Supplementary Fig. 9**), which potentially cause π–cation or electrostatic interactions (Gomes and Shorter 2019; Wang et al. 2018). Deletion analysis showed that a region with basic amino acids (BAA) in the Jas domain is required for frequent eCFP–JAZ2 condensation (**Supplementary Fig. 9**). In the case of the FUS protein, Arg is more important than Lys in molecular interactions that cause phase separation in terms of interaction with Tyr and Phe, because the chemical structure of the cationic side chain of Arg delocalises electron clouds, leading to strong directional preferences with aromatic moieties (Wang et al. 2018). Arg-to-Lys substitutions in the Jas domain (Jas^{RtoK}) decreased eCFP–JAZ2 condensation, in the context of size and frequency, although the secondary structure of the Jas domain might not be affected (**Supplementary Figs. 9, 10**). In contrast, substituting Lys and Arg with Ala in the Jas domain ($Jas^{K,RtoA}$) formed apparent and even larger condensates in the cytosol (**Supplementary Figs. 9, 10**). These results suggest that condensation with partial Jas domain depends

on molecular interactions involving Arg in the Jas domain, and can be replaced by interactions other than π–cation or electrostatic interactions.

JAZ9 can be incorporated into JAZ2 condensates

Since the TIFY and Jas domains are involved in JAZ2 condensation, possibly by interactions between JAZ2 molecules, or JAZ2 and other possible JAZ2 condensate components, if any, we wondered if JAZ9 carrying the conserved domains (Toda et al. 2013; Hori et al. 2014) might be associated with JAZ2 condensates, even though JAZ9 itself does not form condensates as described above. To test this possibility, eCFP-JAZ9 was co-expressed with eYFP–JAZ2 in *O. sativa* protoplasts. This resulted in CFP foci of eCFP–JAZ9, which co-localised with eYFP–JAZ2 condensates in both the nucleus and cytosol (**Fig. 4A**). Such eCFP–JAZ9 and eYFP–JAZ2 co-condensation was observed in most cells with eYFP–JAZ2 condensates (90%, n=10). Thus, JAZ9 may be incorporated into the JAZ2 condensates. Moreover, the CFP signals of eCFP–JAZ9 were more prominent when expressed with eYFP–JAZ2, suggesting that JAZ9 association with JAZ2 condensates represses JAZ9 degradation.

TIFY and Jas domains as well as LCRs cooperatively contribute to JAZ2 condensation

We further examined whether partial JAZ2, such as TIFY–LCR2 or LCR5–Jas, was sufficient for incorporation into the JAZ2 condensate. When co-expressed with eCFP–JAZ2, eYFP-fused TIFY–LCR2 and LCR5–Jas co-localised with eCFP–JAZ2 condensates (**Fig. 4B**). eYFP–TIFY–LCR2 or eYFP–LCR5–Jas co-expression occasionally affected JAZ2 condensation (**Supplementary Fig. 11A**). eYFP–TIFY–LCR2 and eYFP–LCR5–Jas co-condensed with eCFP–JAZ2 in 75–100% and 29–38% cells containing eCFP–JAZ2 condensates, respectively, (**Supplementary Fig. 11A**). This indicates that both regions contain interaction sites between JAZ2 molecules (or other possible components of the JAZ2 condensates).

In contrast, eYFP–LCR5–Jas or eYFP–TIFY–LCR2 scarcely formed condensates when expressed alone (**Supplementary Figs. 11B, C**), suggesting that the TIFY or Jas domain alone does not sufficiently account for the condensate-forming propensity of JAZ2. Moreover, the combined expression of eYFP–LCR5–Jas and eYFP–TIFY–LCR2 did not form condensates (**Supplementary Fig. 11D**). Together with the results of the deletion analyses, these results suggest that the TIFY or Jas domains more likely contribute to JAZ2 condensation cooperatively with other regions.

JAZ2 forms condensates in *N. benthamiana*

We expressed eCFP-JAZ2 in *N. benthamiana*, to find out if JAZ2 forms condensates depending on the cellular environment and experimental conditions. We also thought that if JAZ2 could form condensates in *N. benthamiana*, which is often used for the production of proteins of interest, we would be able to use condensates for engineering in the future. eCFP–JAZ2 foci were found in *N. benthamiana* leaf epidermal cells after transient eCFP–JAZ2 expression by *Agrobacterium* infiltration methods, similarly in *O. sativa* protoplasts (**Fig. 5**). In contrast, no foci were detected with eYFP, which was localised in the nucleus and cytosol (**Fig. 5**), and the control eCFP without fusion to JAZ2 (**Supplementary Fig. 12**). In cells co-expressing eCFP–JAZ2 and eYFP, YFP signals were often excluded at the site of JAZ2 foci, indicating that interaction between the GFP derivatives (eCFP and eYFP) is not necessary for JAZ2 condensate formation. These results suggest that JAZ2 condensation does not require other components specific to *O. sativa* leaf cells than OsJAZ2 and experimental procedure for protoplast transient assays, including PEG-mediated transfection of DNA. Interestingly, however, the JAZ2 condensates differed between the two experimental systems in terms of size and localisation. The diameter of eCFP–JAZ2 condensates found in *N. benthamiana* leaf epidermal cells were 1–4 μm. The smaller (up to 3 μm) condensates were mostly spherical or ellipsoidal, whereas larger condensates (approximately 4 μm) often formed indefinite shapes. They were mostly localised

in the nucleus and occasionally in the vicinity of the nucleus **(Fig. 5)**. However, unlike *O. sativa* protoplasts, JAZ2 condensates in the cytoplasm were not observed at sites distant from the nucleus.

Different properties of JAZ2 condensates in *O. sativa* and *N. benthamiana*

Next, eCFP–JAZ2 molecule fluidity in the JAZ2 condensates was examined by fluorescence recovery after photobleaching (FRAP), which assessed unbleached eCFP–JAZ2 redistribution into the bleached area. In most cases, CFP fluorescence was only slightly recovered after bleaching in *O. sativa* protoplasts, indicating the low mobility of eCFP–JAZ2 molecules **(Fig. 6A and Supplementary Fig. 13A)**. These results suggest that JAZ2 mostly forms gel-like or solid condensates in the *O. sativa* cells. However, in some cases, moderate but apparently higher fluorescence recovery was observed, indicating an increase in the mobile fraction of the condensates (**Figs. 6B–C**). Noticeably, after bleaching of a portion of the JAZ2 condensate, fluorescence increases in the bleached area occurred concomitantly with fluorescence decrease in the unbleached area of the same condensate (**Fig. 6C**), suggesting the exchange of eCFP–JAZ2 molecules between these areas. Therefore, it is most likely that JAZ2 condensates can also adopt a liquid-like state. The difference in the degree of fluorescence recovery seems to be cell-dependent but not size- or condensate localisation-related (**Figs. 6D–E)**.

We expected that the material properties of the JAZ2 condensate might change if the interactions contributing to condensation are compromised. We, therefore, examined the effects of deletion or substitution of potential interacting domains or regions on the molecular fluidity of JAZ2 condensates. Interestingly, fluorescence recovery was moderately increased when condensates formed by eCFP–JAZ2ΔNterm and eCFP–JAZ2ΔTIFY were bleached (**Fig. 6F, Supplementary Fig. 13B**). Unlike this, fluorescence recovery between the condensates formed by eCFP–JAZ2 and other variants, such as JAZ2-Jas^{RtoK}, and JAZ2-Jas^{K,RtoA}, were similar (**Supplementary Fig. 13C**).

In contrast, JAZ2 condensates exhibited substantial levels of fluorescence recovery in *N.*

benthamiana leaf cells, indicating improved eCFP–JAZ2 mobility (**Fig. 6F**). This suggests that JAZ2 forms liquid-like compartments in *N. benthamiana* cells. The liquidity of JAZ2 condensates might be caused by lower levels of eCFP–JAZ2 expression in *N. benthamiana* cells than in *O. sativa* protoplasts. We, therefore, examined FRAP of eCFP–JAZ2 condensates in *O. sativa* protoplasts transfected with lower amounts of plasmid DNA, carrying CaMV 35S promoter::eCFP–JAZ2. The formation of JAZ2 condensates was observed when the amount of plasmid used for the transfection was reduced from 5 μg to 2 μg, but not with 1 μg (**Supplementary Fig. 14A**). Even under the condition of 2 μg, JAZ2 condensates did not exhibit significant fluorescence recovery in *O. sativa* protoplasts (**Supplementary Fig. 14B**). Therefore, it seems unlikely that the liquidity of JAZ2 condensation is caused simply by low levels of JAZ2 expression. Thus, the properties of JAZ2 condensates differ between *O. sativa* and *N. benthamiana*.

JAZ2 forms condensates *in vitro*

Recombinant GFP–JAZ2 was prepared to test whether JAZ2 itself has the propensity to form condensates. The RRM domain and PrLD of the *Arabidopsis* FCA protein (Fang et al. 2019) were used for the control experiments. PrLD, but not the RRM domain of FCA, undergoes phase separation both *in vitro* and *in vivo* (Fang et al. 2019). GFP–JAZ2, GFP–FCA (RRM), GFP–FCA (PrLD), and GFP alone were expressed in *E. coli.,* as soluble proteins by fusion with MBP-tag, and purified by specific binding of MBP-tag to amylose-resin and subsequent elution by maltose **(Supplementary Fig. 15**). GFP–JAZ2 condensation began within 1 h after MBP-tag removal by digestion using TEV protease **(Figs. 7A–D, Supplementary Fig. 15)**. Approximately 0.1–0.3 μM GFP–JAZ2 caused condensation *in vitro* (**Fig. 7, Supplementary Fig. 15**). Under the same experimental conditions, GFP condensation was observed with GFP–FCA (PrLD) even at low levels, but was scarcely or not detected with GFP–FCA (RRM) and GFP alone (**Fig. 7, Supplementary Fig. 15**). Thus, JAZ2 were able to

form condensates outside of plant cells, although the recombinant proteins were not completely pure in these analyses (**Fig. 7C, Supplementary Figs. 15B, C**). These results suggest that JAZ2 is condensate-prone.

The fluidity of GFP–JAZ2 molecules in JAZ2 condensates *in vitro* was examined using FRAP. The GFP signals were not recovered after GFP–JAZ2 condensate photobleaching, suggesting that JAZ2 forms gel-like or solid condensates under the experimental conditions (**Fig. 7E**). Consistent with this, increased incubation of recombinant GFP–JAZ2 *in vitro* formed large, non-spherical, or non-ellipsoidal condensates and occasionally formed massive intricate condensates (**Supplementary Figs. 16A, B**). In the presence of 0.5 M NaCl, JAZ2 condensate formation drastically decreased (**Supplementary Figs. 16C, D**), which is consistent with the possibility that electrostatic and/or π–cation interactions are important for JAZ2 condensation. In contrast, treatment with 1,6-hexanediol, which inhibits weak hydrophobic interactions (Kroschwald, et al. 2017), had little effect on the stability of the JAZ2 condensates formed *in vitro* **(Supplementary Fig. 16E**), as in the experiments using *O. sativa* protoplasts.

Discussion

This study showed that OsJAZ2 is condensation-prone and eCFP–JAZ2 expression causes condensation in *O. sativa* and *N. benthamiana* leaf cell nucleus and cytosol, in addition to typical protein localisation in the nucleus. JAZ2 condensates formed subcellular compartments that excluded mRFP1 and eYFP markers in *O. sativa* and *N. benthamiana*, respectively. Several properties of JAZ2 are similar to those of proteins that play pivotal roles in biomolecular condensate formation via phase separation. Proteins that drive phase separation are often rich in IDR, allowing several conformations and undergoing multivalent interactions among molecules (Banani et al. 2017; Uversky 2017; Peran and Mittag 2020). Similarly, the JAZ2 protein contains IDRs, including PrLD/LCRs, and can form

condensates *in vitro*. Deletion analyses of JAZ2 indicated that the TIFY and Jas domains, as well as LCRs, were involved in condensate formation. The TIFY–LCR2 and LCR5–Jas regions alone were associated with JAZ2 condensates, although each region did not show sufficient proficiency for stable JAZ2 condensate formation. Therefore, these regions may cause multivalent interactions to form JAZ2 condensates.

In this study, JAZ2 frequently formed condensates with varied size, shape, localisation, and molecular fluidity. This might reflect that the structures of the JAZ2 protein and its condensate are metastable, possibly because of multivalent interactions, and can be affected by cellular conditions. Notably, JAZ2 condensates are often larger than *Arabidopsis* FCA condensates, which are spherical with up to approximately 2.5 μm diameter in *Arabidopsis* and tobacco cells (Fang et al. 2019). In contrast, JAZ2 often forms non-spherical condensates that reach 4–7 μm in diameter in *O. sativa* and *N. benthamiana* cells. Such differences in size are likely related to the differences in the nature of the FCA and JAZ2 condensates; FCA forms liquid droplets in *Arabidopsis* and tobacco cells (Fang et al. 2019), whereas JAZ2 forms highly viscous (gel-like or solid) condensates mostly in *O. sativa* protoplasts.

JAZ2 condensate formation frequency was substantially reduced by deleting the Jas domain and adjacent sequence, and substituting four Arg residues in the Jas domain with Lys residues. However, the JAZ2 condensates with the Arg-to-Lys substitution were still solid. This suggests that intermolecular interactions involving Arg residues in the Jas domain, such as π–cation interactions, contribute to JAZ2 condensation process; however, JAZ2 condensate solidification or stability are supported by interactions involving other amino acids. In contrast, BAA (Arg and Lys) substitution with Ala in the Jas domain did not reduce JAZ2 condensate formation frequency, instead forming large condensates. This suggests that an increase in Ala residues in the Jas domain causes other molecular interactions, such as hydrophobic interactions, rather than π–cation or electrostatic interactions, thus

enhancing JAZ2 condensate formation. Interestingly, an Ala-rich sequence in the H1 helix of the Syrian hamster prion protein, Ala–Gly–Ala–Ala–Ala–Gly–Ala, form a β-sheet in an infectious conformation and cause interactions that lead to amyloid formation, which can be mimicked by an Ala tripeptide *in vitro* (Lundberg et al. 1997; Bauer et al. 2011). Likewise, Ala-rich sequences in the mutated Jas domain may have more effect than hydrophobic interactions.

Amyloids such as amyloid-β and α-synuclein, or those found in prion proteins, are formed by cross-β structures (Lundberg et al. 1997; Balbirnie et al. 2001; Bauer et al. 2011; Nelson et al. 2005; Tuttle et al. 2016; Wälti et al. 2016). Although whether JAZ2 forms an amyloid-like structure in *O. sativa* and *in vitro* is unclear, as in the case of Xvelo, a PrLD-containing IDP that constitutes Balbiani bodies in Xenopus (Boke et al. 2016), β-sheets may be involved in solid JAZ2 condensate formation. Structural prediction showed that the TIFY domain of JAZ2 contains a region that forms an antiparallel β-sheet. Moreover, when most of the TIFY domain was deleted, the JAZ2 variant appeared to form more liquid-like condensates in *O. sativa* protoplasts (**Fig. 6F and Supplementary Fig. 13B**). Another possible amyloid-like structure-forming sequence is the Gln- and Asn-rich PrLD/LCR2 of JAZ2 (**Fig. 2**), since polar Gln- and Asn-rich sequences form stacked β-sheet structures (Balbirnie et al. 2001; Nelson et al. 2005). Notably, LCR2 deletion largely impaired JAZ2 condensation, in addition to that TIFY–LCR2 was efficiently incorporated into JAZ2 condensates. It would be interesting to know if such sequences, together with multivalent interactions, contribute to the solid-state of JAZ2 condensation.

Unlike condensates in *O. sativa* protoplasts, eCFP–JAZ2 formed liquid-like condensates in *N. benthamiana* cells. In FRAP analysis, eCFP–JAZ2 fluorescence recovery after bleaching was detected within 5 s and maintained continuously for 60 s (**Fig. 6G**). This is almost comparable to the time required to recover eGFP- or YFP-fused FCA in *Arabidopsis* and tobacco cells (recovery detected within 5 s and continued for 40 to 70 s; Fang et al. 2019). Interestingly, the fluidity of the eCFP-JAZ2

molecules in the JAZ2 condensates differed between *O. sativa* and *N. benthamiana* probably due to the differences in intracellular environments, such as cell volume, or factors leading to post-translational modifications. Noticeably, FRAP analysis indicated that JAZ2 forms solid condensates *in vitro*, as reported in FUS and RBM14 (Hennig et al. 2015). Recombinant GFP– *Arabidopsis* FCA condensates *in vitro* do not show high FCA–GFP fluidity, though FCA forms liquid-like bodies *in vivo*, suggesting the requirement of additional factors for the liquidity of FCA bodies formed *in vivo* (Fang et al. 2019). Likewise, JAZ2 condensates in *N. benthamiana* cells may contain an additional molecule that increases the molecular fluidity of JAZ2.

As discussed by Alberti and Hyman (2021), it is not easy to distinguish whether high-ordered protein assembly is caused by phase separation or reflects insoluble protein aggregation. Protein aggregates are usually referred to as those with irreversible intermolecular interactions. In contrast, however, a small portion of JAZ2 molecules are mobile in not all but some of the JAZ2 condensates (**Figs. 6B and 6C**). Considering that JAZ2 condensates can adopt not only solid-like but also liquid-like states in the cells, it is plausible that JAZ2 shares some propensities with several scaffold proteins that form both dynamic and non-dynamic biomolecular condensates. Interestingly, some of those condensates are solidified rapidly from liquid-like states (Woodruff et al. 2018). Assembles of *C. elegans* SPD5, the key scaffold protein of the pericentriolar material (PCM), are liquid-like droplets 2 min after formation *in vitro* but converted to solid-like structures 15 min after formation (Woodruff et al. 2017). *In vitro* reconstitution of *oskar* ribonucleoprotein granules, which behave as solids and function in embryonic development in *Drosophila*, also shows liquid-to-solid transition within 30 min (Bose et al. 2022). These observations suggest that the *in vivo* solid condensates are derived from liquid-phase condensates. At present, we cannot distinguish whether solid-like JAZ2 condensates may also arise from liquid-like assemblies or they are formed separately, although small JAZ2 condensates are observed with sphere shapes (e.g. in **Fig. 7B**), which is a criterion to assess phase separation-

mediated condensates (Alberti et al. 2019). Another important point is that the material properties (such as liquid or solid state) of condensates formed by multivalent interactions depend on the pattern of their constituents and the valency of interactions (Alberti et al. 2019). For instance, tethering of FUS LCD to the *oskar* granule causes changes in its material properties; from solid to liquid states (Bose et al. 2022). Oppositely, duplication of the RNA-binding domain of the scaffold protein G3BP1 results in less dynamic stress granules (Yang et al 2020). Notably, in our study, partial deletion of the N-terminal region or TIFY domain of JAZ2 increases the mobile fraction of JAZ2 condensates, even moderately (**Fig. 6E and Supplementary Fig. 13C**). This is consistent with the hypothesis that the JAZ2 condensate formation is also driven by multivalent interaction.

The physiological significance of the JAZ2 condensate in *O. sativa* is currently ambiguous. JAZ2 lacks a conserved COI1 binding site and is unlikely to be degraded depending on the JA signal. Therefore, JAZ2 condensates may play a role in JAZ2 inactivation concentration-dependently. Interestingly, JAZ9 was incorporated into the JAZ2 condensates, thus stabilising JAZ9. In addition, TIFY and Jas domains conserved among JAZ factors are involved in JAZ2 condensation, and TIFY domains mediate dimerisation of some JAZ proteins (Chini et al. 2009), raising the possibility that condensation with JAZ2 would be a mode of storage and/or another way of inactivating JAZ9 and possibly other JAZ factors, similar to storage granules reported in yeast (Laporte et al. 2008; Saad et al. 2017; Franzmann et al. 2018). JAZ factor sequestration may also serve as a stress memory, making cells sensitive to repetitive stress that activates JA signalling. However, JAZ2 expression levels might have been fairly high in our transient assay, whereas the expression levels of *JAZ2* in *O. sativa* plants were relatively low, even though *JAZ2* was induced by JA (RiceXpro; https://ricexpro.dna.affrc.go.jp). Thus, JAZ2 accumulation levels might not be sufficient to form condensates under physiological conditions. Alternatively, the opposite situation may also be possible; such low expression levels could have allowed the condensation-prone propensity of JAZ2, without causing potentially detrimental

effects by condensation. It is also noteworthy that YFP-fused AtJAZ1 and AtJAZ9 form subnuclear bodies, when expressed in *Nicotiana tabacum* leaves through *Agrobacterium*-mediated transient expression (Withers et al. 2012). However, the function of such subnuclear bodies has not yet been elucidated. Further studies should describe the physiological roles of JAZ protein condensation.

Transient gene expression using protoplasts and *Agrobacterium* infiltration-mediated gene expression in *N. bethamiana* has been used for several assays in plants. Our results suggest that the condensation-prone propensity of a protein, such as JAZ2, should decrease substantial concentration in cells or localised areas, and therefore affect the evaluation of activity, for example effector activity in the transcriptional activation assay. The same is true for proteins with mutations that would cause or enhance condensation-prone propensity. This possibility must be considered when creating variant proteins, for example, by genome editing.

It would be tempting if artificial subcellular compartments could be newly designed and constructed using condensation-prone proteins in plant cells. Such synthetic compartments may be applied for orthogonal reaction introduction, storage, and molecule sequestration, filtering, or sensing, as reported in mammals and yeast (Shin and Brangwynne 2017; Pancsa et al. 2019), thereby creating cells with new functions (Hastings and Boeynaems 2021). Designing the desired condensates requires a better understanding of controlling condensation-prone protein properties. For this purpose, JAZ2 with unique features is potentially useful for a model study in plant cells, considering that JAZ2 forms relatively large and stable liquid-like to solid-like condensates depending on the cell state or type. In particular, JAZ2 often produces extremely large condensates in the protoplast cytosol. Moreover, Ala substitution of Arg or Lys in the Jas domain formed even larger condensates, suggesting that the JAZ2 condensate size can be easily modulated. Current studies are focusing on amino acid sequences responsible for controlling not only JAZ2 and/or other protein condensate size, but also their subcellular localisation and molecular fluidity. This would enable the modification of such properties

of other membrane-less organelles, thereby extending the potential uses of artificial membrane-less organelles in plant cells in the future.

Supplementary Information

The online version contains supplementary material available. [Supplementary Files 1,2]

References

Alberti S, Gladfelter A, Mittag T (2019) Considerations and challenges in studying liquid-liquid phase separation and biomolecular condensates. Cell 176:419-434. doi: 10.1016/j.cell.2018.12.035.

Alberti S, Hyman AA (2021) Biomolecular condensates at the nexus of cellular stress, protein aggregation disease and ageing. Nat Rev Mol Cell Biol 22:196-213. doi: 10.1038/s41580-020-00326-6.

Asai S, Ohta K, Yoshioka H (2008) MAPK signaling regulates nitric oxide and NADPH oxidase-dependent oxidative bursts in Nicotiana benthamiana. Plant Cell 20:1390-1406.

Balbirnie M, Grothe R, Eisenberg DS (2001) An amyloid-forming peptide from the yeast prion Sup35 reveals a dehydrated beta-sheet structure for amyloid. Proc Natl Acad Sci U S A 98:2375-2380. doi: 10.1073/pnas.041617698.

Banani SF, Lee HO, Hyman AA et al (2017) Biomolecular condensates: organizers of cellular biochemistry. Nat Rev Mol Cell Biol 18:285-298.

Bauer MT, Gilmore KA, Petty SA (2011) Formation of β-sheets in glutamine and alanine tripeptides. Biochem Biophys Res Commun 406:348-352. https://doi.org/10.1016/j.bbrc.2011.02.041.

Boke E, Ruer M, Wühr M et al (2016) Amyloid-like self-assembly of a cellular compartment. Cell 166:637-650. https://doi.org/10.1016/j.cell.2016.06.051

Bose M, Lampe M, Mahamid J et al (2022) Liquid-to-solid phase transition of *oskar* ribonucleoprotein granules is essential for their function in *Drosophila* embryonic development. Cell 185:1308-1324. doi: 10.1016/j.cell.2022.02.022.

Chini A, Fonseca S, Chico JM et al (2009) The ZIM domain mediates homo- and heteromeric interactions between Arabidopsis JAZ proteins. Plant J 59:77–87.

Chini A, Gimenez-Ibanez S, Goossens A et al (2016) Redundancy and specificity in jasmonate signalling. Curr Opin Plant Biol 33:147-156. doi: 10.1016/j.pbi.2016.07.005.

Courchaine EM, Lu A, Neugebauer KM. Droplet organelles? (2016) EMBO J 35:1603-1612. doi: 10.15252/embj.201593517.

Fang X, Wang L, Ishikawa R et al (2019) Arabidopsis FLL2 promotes liquid-liquid phase separation of polyadenylation complexes. Nature 569:265-269. doi: 10.1038/s41586-019-1165-8.

Franzmann TM, Jahnel M, Pozniakovsky A et al (2018). Phase separation of a yeast prion protein promotes cellular fitness. Science 359:eaao5654. doi: 10.1126/science.aao5654.

Garabedian MV, Wang W, Dabdoub JB et al (2021) Designer membraneless organelles sequester native factors for control of cell behavior. Nat Chem Biol 17:998–1007. doi: 10.1038/s41589-021-00840-4.

Garbuzynskiy SO, Lobanov MY, Galzitskaya OV (2010) FoldAmyloid: a method of prediction of amyloidogenic regions from protein sequence. Bioinformatics 26:326-332. doi: 10.1093/bioinformatics/btp691.

Gomes E, Shorter J (2019) The molecular language of membraneless organelles. J Biol Chem 294:7115-7127. doi:10.1074/jbc.TM118.001192

Hastings RL, Boeynaems S (2021) Designer Condensates: A toolkit for the biomolecular architect. J Mol Biol 433:166837.

Hellens RP, Edwards EA, Leyland NR et al (2000) pGreen: a versatile and flexible binary Ti vector

for Agrobacterium-mediated plant transformation. Plant Mol Biol 42:819-32. doi: 10.1023/a:1006496308160. PMID: 10890530.

Hennig S, Kong G, Mannen T et al (2015) Prion-like domains in RNA binding proteins are essential for building subnuclear paraspeckles. J Cell Biol 210:529-39. doi: 10.1083/jcb.201504117.

Hori Y, Kurotani K, Toda Y et al (2014). Overexpression of the JAZ factors with mutated jas domains causes pleiotropic defects in rice spikelet development. Plant Signal Behav 9:e970414. doi: 10.4161/15592316.2014.970414.

Howe GA, Major IT, Koo AJ (2018) Modularity in jasmonate signaling for multistress resilience. Annu Rev Plant Biol 69:387-415. doi: 10.1146/annurev-arplant-042817-040047.

Huang H, Liu B, Liu L et al (2017) Jasmonate action in plant growth and development. J Exp Bot 68:1349-1359. doi: 10.1093/jxb/erw495.

Hughes MP, Sawaya MR, Boyer DR et al (2018) Atomic structures of low-complexity protein segments reveal kinked β sheets that assemble networks. Science 359:698-701. doi: 10.1126/science.aan6398.

Jumper J, Evans R, Pritzel A et al (2021) Highly accurate protein structure prediction with AlphaFold. Nature 596:583-589. doi: 10.1038/s41586-021-03819-2

Kato M, Han TW, Xie S et al (2012) Cell-free formation of RNA granules: low complexity sequence domains form dynamic fibers within hydrogels. Cell 149:753-767.

Kroschwald S, Maharana S, Mateju D et al (2015) Promiscuous interactions and protein disaggregates determine the material state of stress-inducible RNP granules. Elife 4:e06807. doi: 10.7554/eLife.06807.

Kroschwald S, Maharana S, Alberti S (2017) Hexanediol: a chemical probe to investigate the material properties of membrane-less compartments. Matters doi: 10.19185/matters.201702000010

Kurotani K, Hayashi K, Hatanaka S et al (2015) Elevated levels of CYP94 family gene expression

alleviate the jasmonate response and enhance salt tolerance in rice. Plant Cell Physiol 56:779-789. doi: 10.1093/pcp/pcv006.

Laporte D, Salin B, Daignan-Fornier B et al (2008) Reversible cytoplasmic localization of the proteasome in quiescent yeast cells. J Cell Biol 181:737-745. doi: 10.1083/jcb.200711154.

Lin Y, Protter DS, Rosen MK et al (2015) Formation and Maturation of Phase-Separated LiquidDroplets by RNA-Binding Proteins. Mol Cell 60:208-219. https://doi.org/10.1016/j.molcel.2015.08.018.

Lundberg KM, Stenland CJ, Cohen FE et al (1997) Kinetics and mechanism of amyloid formation by the prion protein H1 peptide as determined by time-dependent ESR. Chemistry & Biology 4:345-355. https://doi.org/10.1016/S1074-5521(97)90125-3.

Mirdita M, Schütze K, Moriwaki Y et al (2021) ColabFold - Making protein folding accessible to all. bioRxiv. doi: 10.1101/2021.08.15.456425

Molliex A, Temirov J, Lee J et al (2015) Phase separation by low complexity domains promotes stress granule assembly and drives pathological fibrillization. Cell 163:123-133.

Motohashi K (2015) A simple and efficient seamless DNA cloning method using SLiCE from Escherichia coli laboratory strains and its application to SLiP site-directed mutagenesis. BMC Biotechnol 15:47. doi: 10.1186/s12896-015-0162-8.

Nelson R, Sawaya MR, Balbirnie M et al (2005) Structure of the cross-beta spine of amyloid-like fibrils. Nature 435:773-778. doi: 10.1038/nature03680.

Niepel M, Gallie DR (1999) Identification and characterization of the functional elements within the tobacco etch virus 5' leader required for cap-independent translation. J Virol 73:9080-9088. doi: 10.1128/JVI.73.11.9080-9088.1999.

Ogawa D, Suzuki Y, Yokoo T et al (2021) Acetic-acid-induced jasmonate signaling in root enhances drought avoidance in rice. Sci Rep 11:6280. doi: 10.1038/s41598-021-85355-7.

Ohira K, Ojima K, Fujiwara A (1973) Studies on the nutrition of rice cell culture I. A simple, defined medium for rapid growth in suspension culture. Plant Cell Physiol 14: 1113–1121. https://doi.org/10.1093/oxfordjournals.pcp.a074950

Pancsa R, Schad E, Tantos A et al (2019) Emergent functions of proteins in non-stoichiometric supramolecular assemblies. Biochim Biophys Acta Proteins Proteom 1867:970-979. doi: 10.1016/j.bbapap.2019.02.007.

Patel A, Lee HO, Jawerth L et al (2015) A liquid-to-solid phase transition of the ALS protein FUS accelerated by disease mutation. Cell 162:1066-1077.

Peran I, Mittag T (2020) Molecular structure in biomolecular condensates. Curr Opin Struct Biol 60: 17-26. https://doi.org/10.1016/j.sbi.2019.09.007

Reinkemeier CD, Girona GE, Lemke EA (2019) Designer membraneless organelles enable codon reassignment of selected mRNAs in eukaryotes. Science 363:eaaw2644. doi: 10.1126/science.aaw2644. PMID: 30923194.

Saad S, Cereghetti G, Feng Y et al (2017) Reversible protein aggregation is a protective mechanism to ensure cell cycle restart after stress. Nat Cell Biol 19:1202-1213. doi: 10.1038/ncb3600.

Segami S, Makino S, Miyake A et al (2014) Dynamics of vacuoles and H+-pyrophosphatase visualized by monomeric green fluorescent protein in Arabidopsis: artifactual bulbs and native intravacuolar spherical structures. Plant Cell 26:3416-3434. doi: 10.1105/tpc.114.127571.

Shin Y, Brangwynne CP (2017) Liquid phase condensation in cell physiology and disease. Science 357:eaaf4382.

Shyu C, Figueroa P, Depew CL et al (2012) JAZ8 lacks a canonical degron and has an EAR motif that mediates transcriptional repression of jasmonate responses in Arabidopsis. Plant Cell 24:536-550. doi: 10.1105/tpc.111.093005.

Toda Y, Tanaka M, Ogawa D et al (2013). RICE SALT SENSITIVE3 forms a ternary complex with

JAZ and class-C bHLH factors and regulates jasmonate-induced gene expression and root cell elongation. Plant Cell 25:1709-1725. doi: 10.1105/tpc.113.112052.

Tuttle MD, Comellas G, Nieuwkoop AJ et al (2016) Solid-state NMR structure of a pathogenic fibril of full-length human α-synuclein. Nat Chem Biol 23:409–415.

Uversky VN (2017) Protein intrinsic disorder-based liquid-liquid phase transitions in biological systems: Complex coacervates and membrane-less organelles. Adv Colloid Interface Sci 239: 97-114. https://doi.org/10.1016/j.cis.2016.05.012

Wälti MA, Ravotti F, Arai H et al (2016) Atomic-resolution structure of a disease-relevant Aβ(1–42) amyloid fibril. Proc Natl Acad Sci USA 113: E4976-E4984. https://doi.org/10.1073/pnas.1600749113

Wang J, Choi J-M, Holehouse AS et al (2018) A Molecular Grammar Governing the Driving Forces for Phase Separation of Prion-like RNA Binding Proteins. Cell 174:688-699. https://doi.org/10.1016/j.cell.2018.06.006.

Wasternack C, Hause B (2013) Jasmonates: biosynthesis, perception, signal transduction and action in plant stress response, growth and development. An update to the 2007 review in Annals of Botany. Ann Bot 111:1021-1058. doi: 10.1093/aob/mct067.

Withers J, Yao J, Mecey C et al (2012) Transcription factor-dependent nuclear localization of a transcriptional repressor in jasmonate hormone signaling. Proc Natl Acad Sci USA 109:20148-20153. doi: 10.1073/pnas.1210054109.

Woodruff JB, Ferreira Gomes B, Widlund PO, et al (2017) The centrosome is a selective condensate that nucleates microtubules by concentrating tubulin. Cell 169:1066-1077. doi: 10.1016/j.cell.2017.05.028.

Woodruff JB, Hyman AA, Boke E (2018) Organization and function of non-dynamic biomolecular condensates. Trends Biochem Sci 43:81-94. doi: 10.1016/j.tibs.2017.11.005.

Wu H, Ye H, Yao R et al (2015) OsJAZ9 acts as a transcriptional regulator in jasmonate signaling and modulates salt stress tolerance in rice. Plant Sci232:1-12. doi: 10.1016/j.plantsci.2014.12.010.

Yang P, Mathieu C, Kolaitis RM et al (2020) G3BP1 is a tunable switch that triggers phase separation to assemble stress granules. Cell 181:325-345. doi: 10.1016/j.cell.2020.03.046.

Zacharias DA, Violin JD, Newton AC et al (2002) Partitioning of lipid-modified monomeric GFPs into membrane microdomains of live cells. Science 296:913-916. doi: 10.1126/science.1068539.

Statements and Declarations

Funding

This work was partially supported by the Japan Society for the Promotion of Science (JSPS) KAKENHI (JP16K08140 and JP22K05427) and Nagoya University–National Institute of Advanced Industrial Science and Technology (NU-AIST) alliance project. YK was supported by the Japan Science and Technology Agency (JST) SPRING (JPMJSP2125) and "Graduate Program of Transformative Chem-Bio Research" in Nagoya University, supported by The Ministry of Education, Culture, Sports, Science and Technology (MEXT) (WISE Program).

Competing Interests

The authors have no relevant financial or non-financial interests to disclose.

Author Contributions

All authors contributed to the study conception and/or design. Material preparation, data collection and analysis were performed by YK, YJ, TA, YY, HG, NH, and HK. OsJAZ2 condensation in *Oryza sativa* cells was first reported by HK. Data interpretation was performed by TH and ST in addition to the authors described above. The first draft of the manuscript was written by YK and ST and improved

by the other authors' suggestions. All authors read and approved the final manuscript.

Data Availability

The datasets generated during and/or analysed during the current study are available from the corresponding author on reasonable request.

Figure Legends

Fig. 1 OsJAZ2 frequently forms condensates in *Oryza sativa* protoplasts

(A) Top, schematic domain structure of OsJAZ2. TIFY and Jas domains, EAR motif, and five low-complexity regions (LCRs) are depicted. Bottom, prion-like domain (PrLD) and intrinsically disordered regions (IDRs) are predicted by 'Prion-like Amino Acid Composition' (PLAAC; http://plaac.wi.mit.edu/) and 'Database of Disordered Protein Prediction' (D^2P^2; https://d2p2.pro/) algorithms, respectively. **(B)** Fluorescence microscopy of *O. sativa* protoplasts expressing eCFP–JAZ2, eYFP–bHLH094, and mRFP1. CFP, YFP, and RFP images are shown with pseudo-colours. Subcellular localisation of eCFP–JAZ2 (I) without or (II–V) with CFP foci in five representative cells is shown. The JAZ2 condensate and nucleus positions are indicated by white and orange arrowheads, respectively. I, no JAZ2 condensate but nuclear localisation of JAZ2. II and III, JAZ2 condensates present in the vicinity of the nucleus. IV and V, large JAZ2 condensates in the vicinity of the nucleus and in the cytosol, respectively. eYFP–bHLH094 and mRFP1 were co-expressed for visualisation of the nucleus (YFP) and both the nucleus and cytosol (RFP), respectively. In images I and II, cells with large vacuoles (vac) are shown. The position of JAZ2 foci shown in II is devoid of RFP signals. Scale bars, 5 μm. **(C)** Z-stack image set of the nucleus in the cell shown in **B** (**panel II**) and **Supplementary Fig. 3B**. Images of CFP (top) and YFP (middle) of the same nucleus are merged (bottom). White arrowheads indicate typical eCFP–JAZ2 condensates formed in the nucleus. The position of the focal

plane on the z-axis is shown in the top panels. The images were obtained with an 100× objective lens. Scale bars, 1 μm.

Fig. 2 Prediction of amyloidogenic regions and eCFP–JAZ2 3-D structure.

(A) Amino acid sequence of the eCFP–JAZ2 fusion protein was analysed by the FoldAmyloid program (http://bioinfo.protres.ru/fold-amyloid/). Amino acids marked in blue-violet indicate sequences prone to amyloid-like aggregation. Amino acid sequences of eCFP and JAZ2 are boxed. EAR motif, TIFY, and Jas domain are indicated by blue, red, and yellow underlines, respectively. The sequence predicted as JAZ2–PrLD (see **Fig. 1**) is indicated by a green underline.

(B) Prediction of the three-dimensional structure of eCFP-JAZ2 by Alphafold2 (https://colab.research.google.com/github/sokrypton/ColabFold/blob/main/AlphaFold2.ipynb) (Mirdita et al. 2021; Jumper et al.2021). Blue and red indicate regions of high and low confidence, respectively. The black arrow indicates the position of the TIFY domain of JAZ2. The secondary JAZ2 structure was predicted as also shown in **Supplementary Fig. 10A**

Fig. 3 TIFY and Jas domains are required for stable JAZ2 condensate formation

(A) Deletion constructs of OsJAZ2 used for condensation assay in *Oryza sativa* protoplasts. TIFY and Jas domains, EAR motif, and low-complexity regions (LCRs) are depicted as in **Fig. 1A**. The position of amino acid is indicated. **(B)** Frequency of JAZ2 condensate formation. The rate of cells with and without JAZ2 condensate formation by expression of eCFP-fused constructs indicated in (A) with eYFP–bHLH094 and mRFP1 in *O. sativa* protoplasts are shown (n = 10–15). Similar results, except for the effects of N-terminal region deletion, are shown in **Supplementary Fig. 7**

Fig. 4 Proteins carrying TIFY and Jas domains are associated with JAZ2 condensates

(A) Top, *Oryza sativa* protoplasts expressing (left) eCFP–JAZ9 and (right) eYFP–JAZ2, with mRFP1, respectively. Bottom, two representative *O. sativa* protoplasts co-expressing eCFP–JAZ9 and eYFP–JAZ2 with mRFP1. CFP, YFP, and RFP images and merged images are shown with pseudo-colours. **(B)** Top, schematic structure of truncated OsJAZ2 proteins, (left) TIFY–LCR2 and (right) LCR5–Jas fused to eYFP. Bottom, *O. sativa* protoplasts co-expressing (upper panels) eYFP–TIFY–LCR2 or (lower panels) eYFP–LCR5–Jas with eCFP-JAZ2 and mRFP1, respectively. The positions of typical JAZ2 condensates and the nucleus are indicated by white and orange arrowheads, respectively. (A) eCFP–JAZ9 foci, (B) eYFP–TIFY–LCR2 and eYFP–LCR5–Jas are co-localized with JAZ2 condensates. mRFP1 visualizes both the nucleus and cytosol (RFP). Scale bars, 5 μm

Fig. 5 OsJAZ2 forms condensates in *Nicotiana benthamiana*

Fluorescence microscopy of *N. benthamiana* leaf epidermal cells co-expressing eCFP–JAZ2 and eYFP. The CFP and YFP images are shown in pseudo-colours. (I–III) The subcellular localisation of eCFP–JAZ2 with JAZ2 foci in three representative cells is shown. Magnified views of the nucleus and its vicinity are shown beneath the respective cell panels. The positions of the JAZ2 condensates and nuclei are indicated by white and orange arrows, respectively. I: Nuclear localisation of JAZ2 with JAZ2 condensates. II, Nuclear localisation of JAZ2 with JAZ2 condensates in the vicinity of the nucleus. III, large JAZ2 condensates in the nucleus. eYFP visualises both the nucleus and the cytosol. Scale bars, 30 μm

Fig. 6 Fluorescence recovery after photobleaching (FRAP) of eCFP–JAZ2 condensates

(A, B) Top, representative images of eCFP–JAZ2 condensates in the nuclei of *Oryza sativa* protoplasts before and after photobleaching, showing (A) no and (B) slight CFP fluorescence recovery. Yellow arrowheads indicate the photobleaching site. Time 0 indicates the time point of the bleaching pulse.

Scale bar, 2 μm. Bottom, the normalised FRAP intensity corresponding to the top images is shown. **(C)** FRAP of an eCFP–JAZ2 condensate after partial bleaching showing slight fluorescence recovery. Top, fluorescence images of an *O. sativa* protoplast expressing eCFP–JAZ2 with eYFP–bHLH094 and mRFP1. The positions of the JAZ2 condensate subjected to FRAP and nuclei are indicated by white and orange arrows, respectively. Middle, fluorescence recovery of eCFP–JAZ2 after photobleaching at the indicated position by yellow arrowheads. Scale bar, 5 μm. Bottom, the normalised fluorescence intensity at the bleached (blue) and unbleached (green) areas in the same condensate. Inset, measurement areas in the bleached (blue) and unbleached (green) areas were indicated. **(D, E)** Normalised fluorescence intensity at 100 s after photobleaching of eCFP–JAZ2 condensates in *O. sativa* protoplasts, classified by JAZ2 condensate (D) size and (E) localisation. In (D), 'small' and 'large' indicate ≤1 μm and >1 μm in diameter, respectively. **(F)** Normalised fluorescence intensity at 100 s after photobleaching of eCFP–JAZ2, eCFP–JAZ2ΔNterm and eCFP–JAZ2ΔTIFY condensates, as shown in **Supplementary Fig. 13B**. **(G)** A representative image of eCFP–JAZ2 condensate in *N. benthamiana* leaf cell nucleus before and after photobleaching (top), and normalised FRAP intensity (bottom). CFP fluorescence intensity at 100 s is shown (mean±SD, n=3). Yellow arrowheads indicate the photobleaching site. Time 0 indicates the time point of the bleaching pulse. Scale bar, 5 μm. An asterisk indicates significance as evaluated by Welch's *t*-test (P <0.05). n.s. means 'not significant'. The image acquisition speed in these FRAP analyses was 2 μs/pixel, except for the analysis in (C), which was 4 μs/pixel. Accordingly, the data in (C) is not included in the comparison in (D-F).

Fig. 7 GFP–JAZ2 condensation *in vitro*

(A) Condensation of recombinant GFP-fused JAZ2, FCA–PrLD and FCA–RRM, and GFP alone. GFP fluorescence of these proteins obtained from MBP-tagged proteins after cleavage with TEV protease for 2 h in the presence of 150 mM NaCl was observed using a confocal laser scanning microscope

(CLSM). Images with two different brightness (top and bottom) are shown. The 1.6-fold volume protein solution analysed by sodium dodecyl sulfate polyacrylamide gel electrophoresis (SDS–PAGE) as in (C) was used for observation. Scale bar, 10 μm. **(B)** (left) GFP fluorescence and (right) differential interference contrast (DIC) images of GFP–JAZ2 condensates *in vitro* as in (A). Typical condensates are indicated by white and black arrows in the GFP and DIC images. Scale bar, 10 μm. **(C)** SDS–PAGE of recombinant GFP-fused JAZ2, FCA–PrLD, FCA–RRM, and GFP alone (closed arrowheads). Estimated concentrations (μM) of GFP-tagged proteins after TEV cleavage are 0.3 (GFP–JAZ2), 0.3 (GFP–FCA–PrLD), 0.1 (GFP–FCA–RRM), and 0.9 (GFP). Open arrowhead indicates the band position of MBP protein obtained after cleavage with TEV protease. **(D)** Recombinant GFP–JAZ2 (~0.5 μM) condensation was obtained from MBP–GFP–JAZ2 after cleavage with TEV protease for the indicated time period in the presence of 100 mM NaCl. Scale bar, 5 μm. **(E)** Fluorescence recovery after photobleaching (FRAP) of GFP–JAZ2 condensates formed *in vitro.* GFP–JAZ2 protein solution (~0.3 μM) was obtained after cleavage with TEV protease in the presence of 100 mM NaCl. (left) Typical GFP images before and after photobleaching. Scale bars, 1 μm. (right) Normalised intensity of GFP fluorescence before and after bleaching (mean±SD, n=5). Note that recombinant proteins were not further purified after TEV cleavage, and the protein solutions used for microscopic observation contained MBP protein and TEV protease

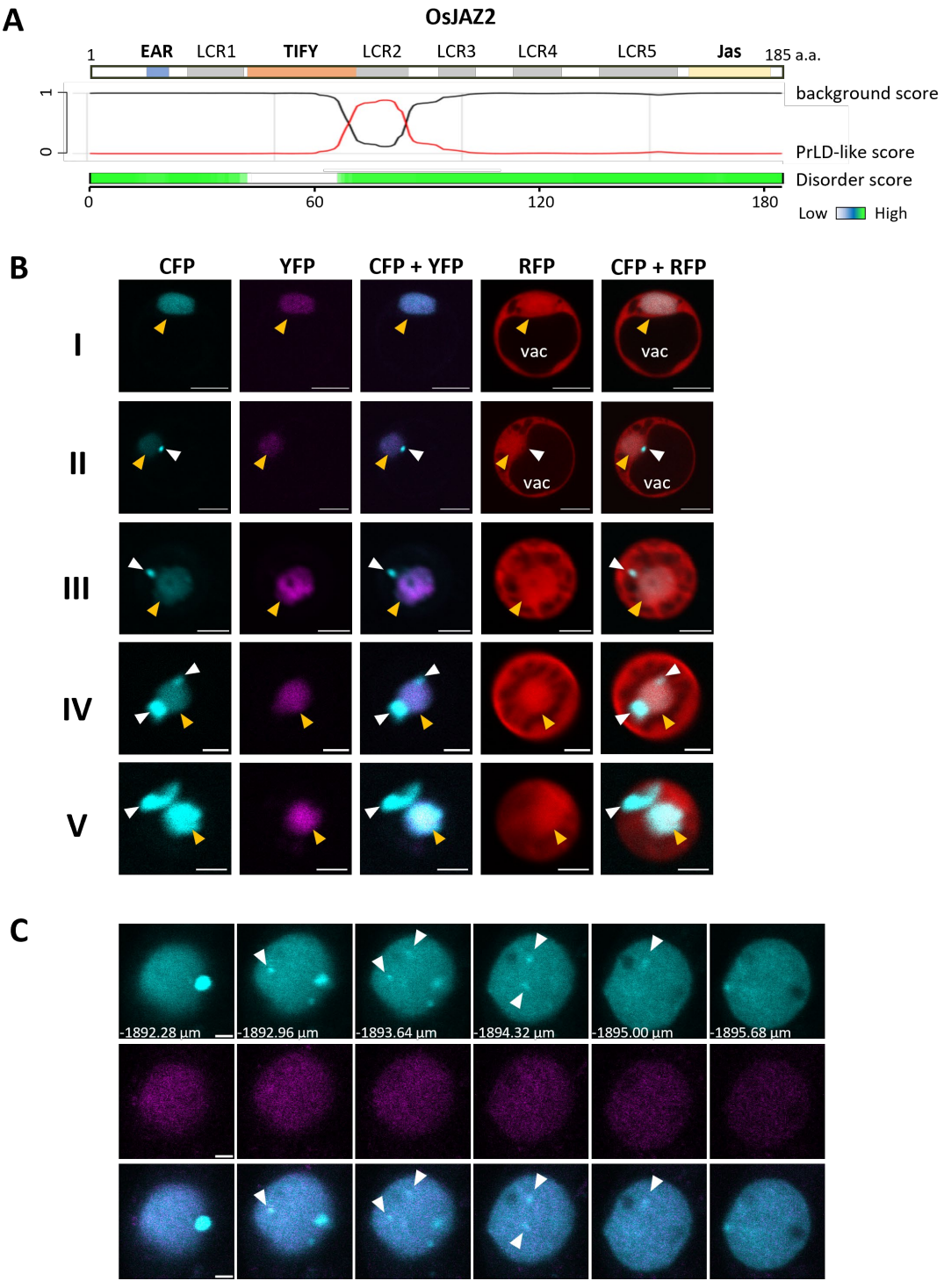
A
OsJAZ2
1
EAR
LCR1
TIFY
LCR2
LCR3
LCR4
LCR5
Jas
185 a.a.
background score
PrLD-like score
Disorder score
Low
High
0
60
120
180
B
CFP
YFP
CFP + YFP
RFP
CFP + RFP
I
II
III
IV
V
vac
C
-1892.28 µm
-1892.96 µm
-1893.64 µm
-1894.32 µm
-1895.00 µm
-1895.68 µm

[Fig. 1]

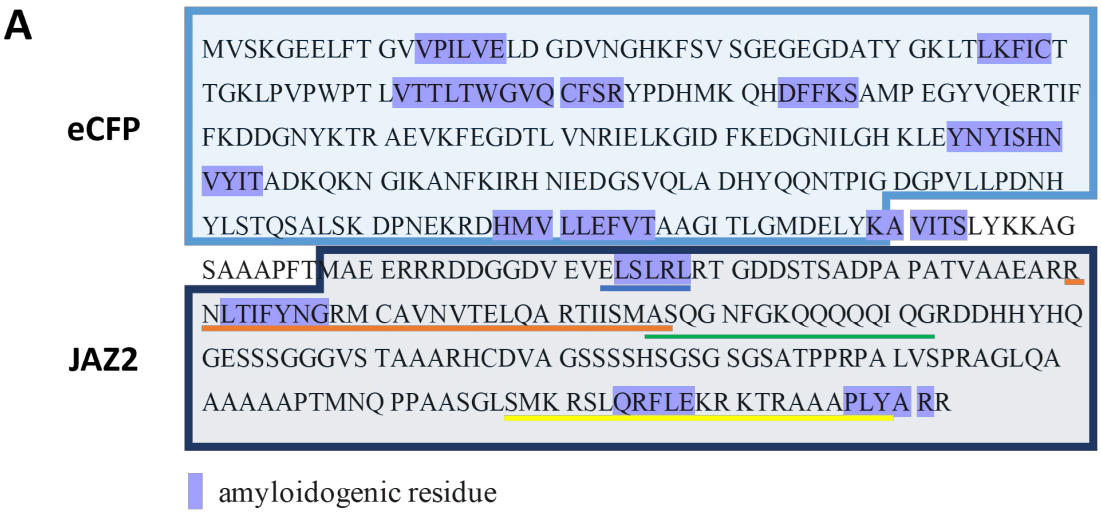
A
eCFP
MVSKGEELFT GVVPILVELD GDVNGHKFSV SGEGEGDATY GKLTLKFICT
TGKLPVPWPT LVTTLTWGVQ CFSRYPDHMK QHDFFKSAMP EGYVQERTIF
FKDDGNYKTR AEVKFEGDTL VNRIELKGID FKEDGNILGH KLEYNYISHN
VYITADKQKN GIKANFKIRH NIEDGSVQLA DHYQQNTPIG DGPVLLPDNH
YLSTQSALSK DPNEKRDHMV LLEFVTAAGI TLGMDELYKA VITSLYKKAG
JAZ2
SAAAPFTMAE ERRRDDGGDV EVELSLRLRT GDDSTSADPA PATVAAEARR
NLTIFYNGRM CAVNVTELQA RTIISMASQG NFGKQQQQQI QGRDDHHYHQ
GESSSGGGVS TAAARHCDVA GSSSSHSGSG SGSATPPRPA LVSPRAGLQA
AAAAAPTMNQ PPAASGLSMK RSLQRFLEKR KTRAAAPLYA RR
amyloidogenic residue

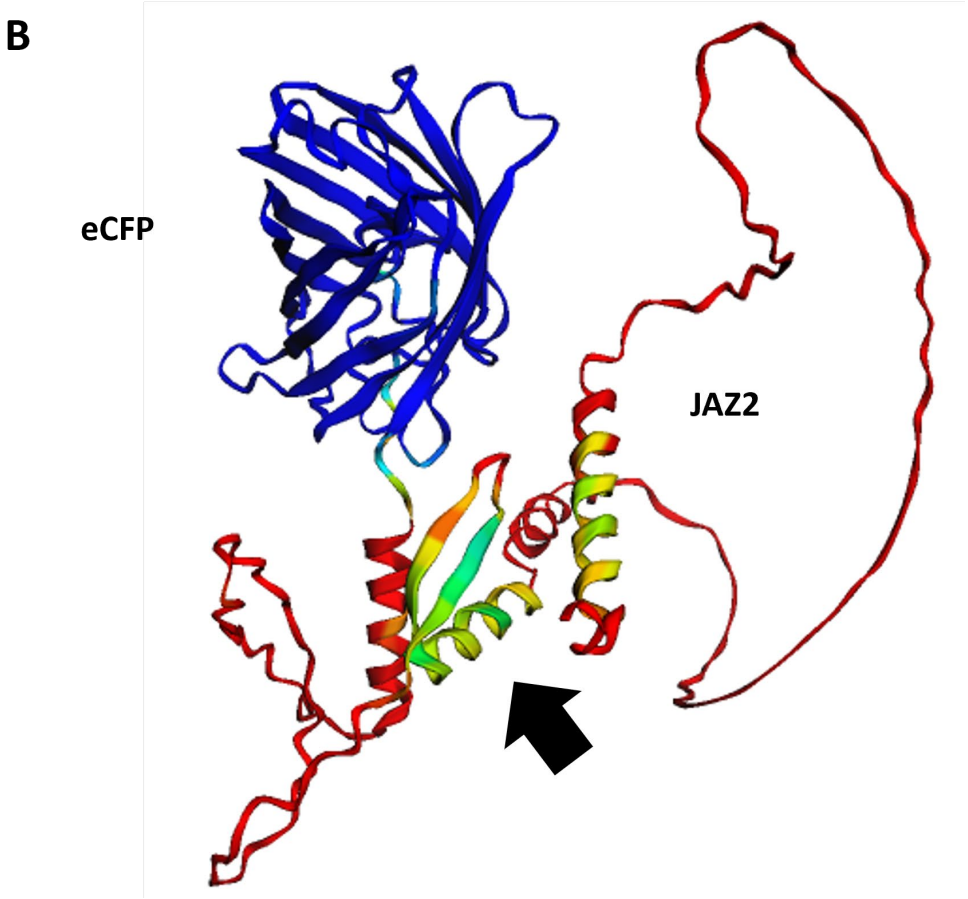
B
eCFP
JAZ2

[Fig. 2]

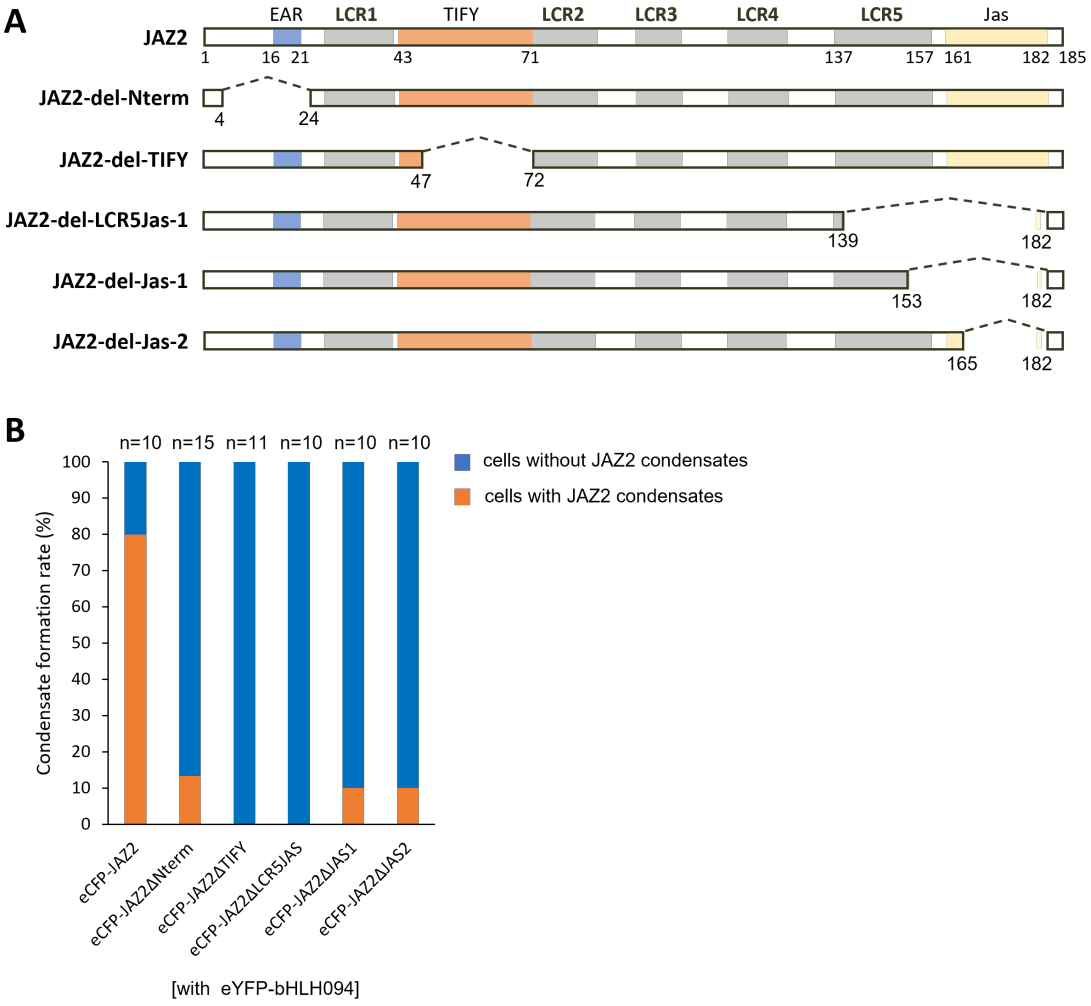
A
EAR
LCR1
TIFY
LCR2
LCR3
LCR4
LCR5
Jas
JAZ2
1
16
21
43
71
137
157
161
182
185
JAZ2-del-Nterm
4
24
JAZ2-del-TIFY
47
72
JAZ2-del-LCR5Jas-1
139
182
JAZ2-del-Jas-1
153
182
JAZ2-del-Jas-2
165
182
B
n=10
n=15
n=11
n=10
n=10
n=10
cells without JAZ2 condensates
cells with JAZ2 condensates
Condensate formation rate (%)
100
90
80
70
60
50
40
30
20
10
0
eCFP-JAZ2
eCFP-JAZ2ΔNterm
eCFP-JAZ2ΔTIFY
eCFP-JAZ2ΔLCR5JAS
eCFP-JAZ2ΔJAS1
eCFP-JAZ2ΔJAS2
[with eYFP-bHLH094]

[Fig. 3]

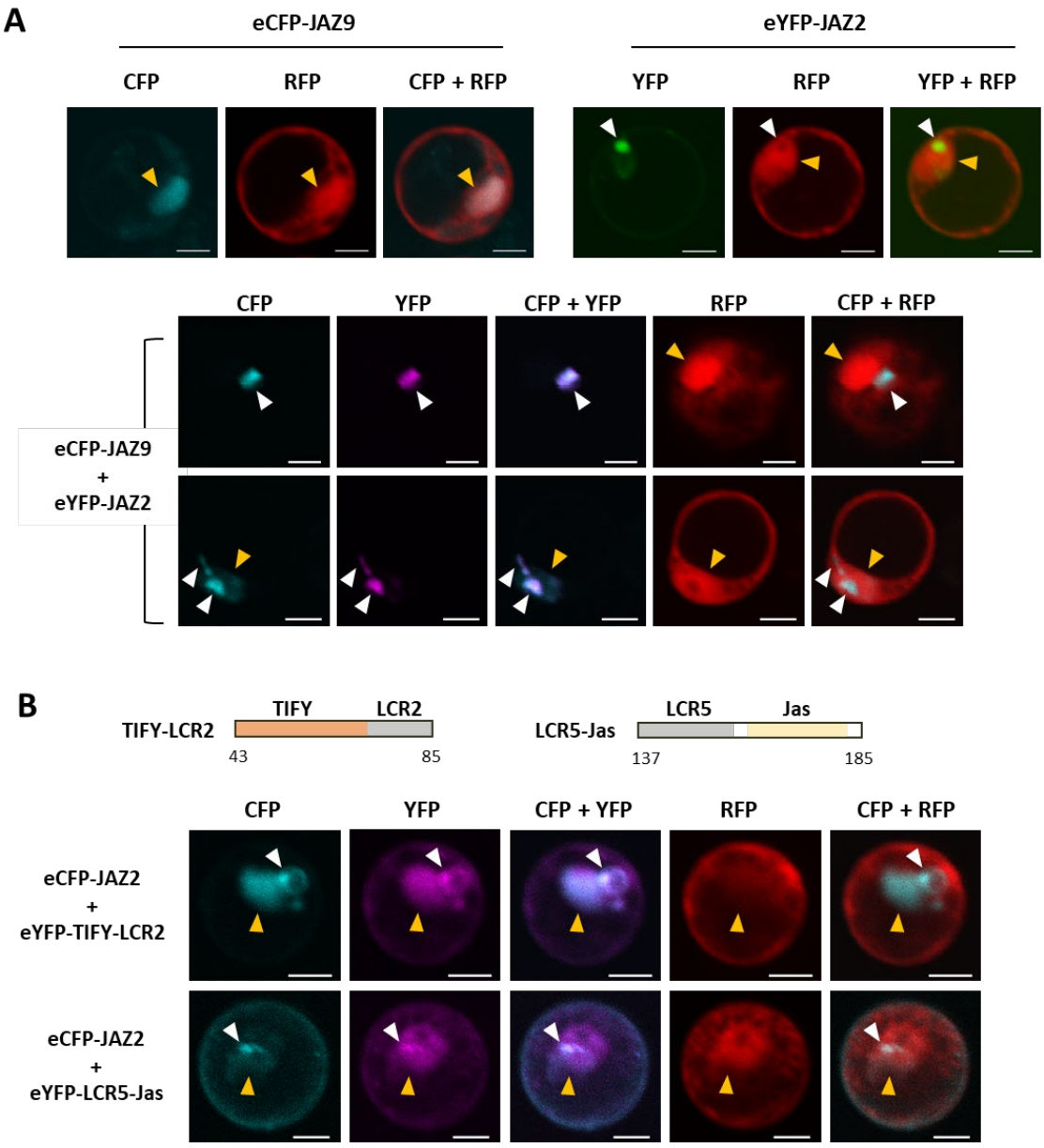
A
eCFP-JAZ9
eYFP-JAZ2
CFP
RFP
CFP + RFP
YFP
RFP
YFP + RFP
CFP
YFP
CFP + YFP
RFP
CFP + RFP
eCFP-JAZ9
+
eYFP-JAZ2
B
TIFY-LCR2
TIFY
LCR2
43
85
LCR5-Jas
LCR5
Jas
137
185
CFP
YFP
CFP + YFP
RFP
CFP + RFP
eCFP-JAZ2
+
eYFP-TIFY-LCR2
eCFP-JAZ2
+
eYFP-LCR5-Jas

[Fig. 4]

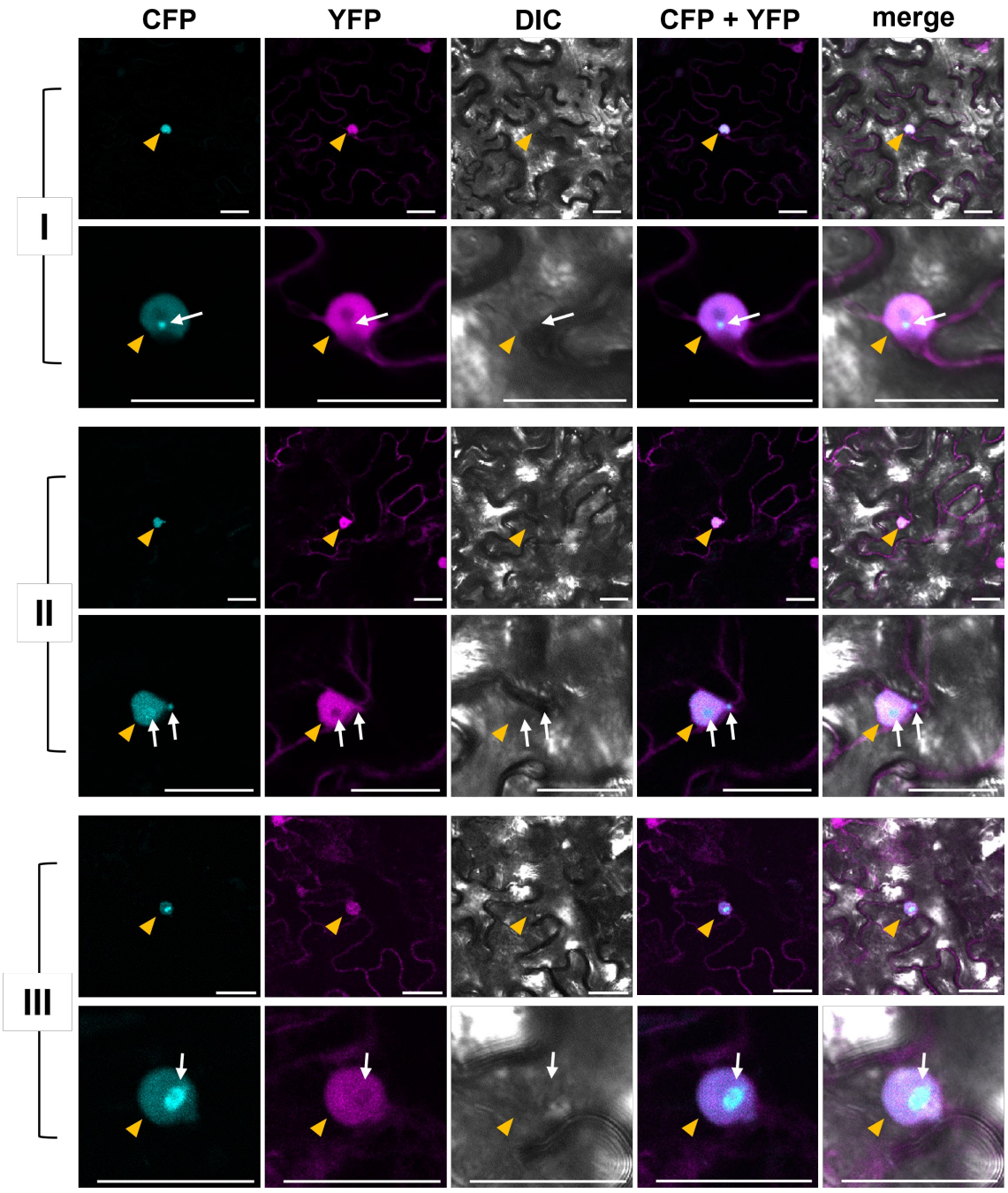

[Fig. 5]

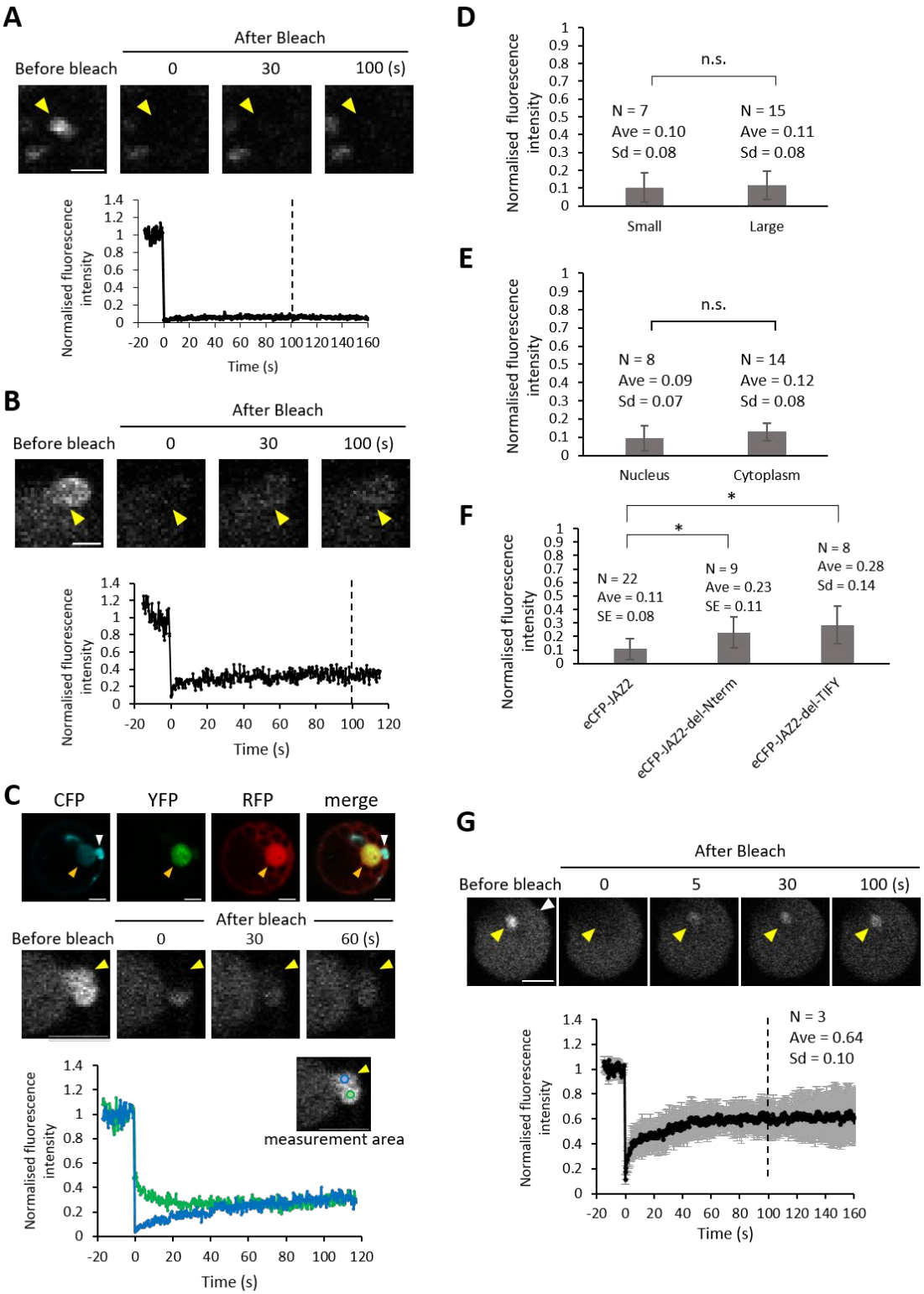
A
After Bleach
Before bleach
0
30
100 (s)
Normalised fluorescence intensity
Time (s)
B
After Bleach
Before bleach
0
30
100 (s)
Normalised fluorescence intensity
Time (s)
C
CFP
YFP
RFP
merge
After bleach
Before bleach
0
30
60 (s)
measurement area
Normalised fluorescence intensity
Time (s)
D
Normalised fluorescence intensity
n.s.
N = 7
Ave = 0.10
Sd = 0.08
N = 15
Ave = 0.11
Sd = 0.08
Small
Large
E
Normalised fluorescence intensity
n.s.
N = 8
Ave = 0.09
Sd = 0.07
N = 14
Ave = 0.12
Sd = 0.08
Nucleus
Cytoplasm
F
Normalised fluorescence intensity
*
*
N = 22
Ave = 0.11
SE = 0.08
N = 9
Ave = 0.23
SE = 0.11
N = 8
Ave = 0.28
Sd = 0.14
eCFP-JAZ2
eCFP-JAZ2-del-Nterm
eCFP-JAZ2-del-TIFY
G
After Bleach
Before bleach
0
5
30
100 (s)
Normalised fluorescence intensity
N = 3
Ave = 0.64
Sd = 0.10
Time (s)

[Fig. 6]

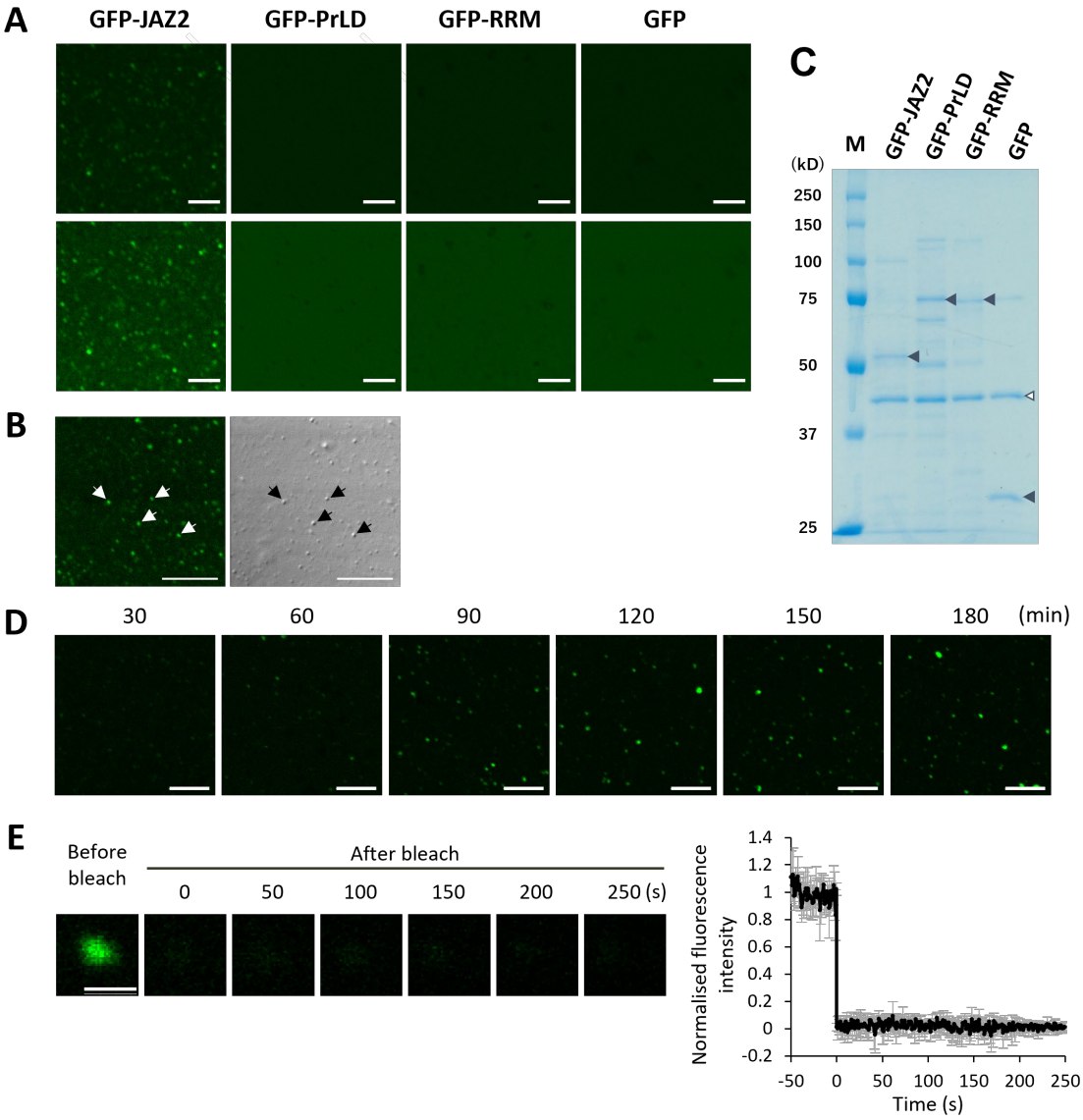
A
GFP-JAZ2
GFP-PrLD
GFP-RRM
GFP
B
C
M
GFP-JAZ2
GFP-PrLD
GFP-RRM
GFP
(kD)
250
150
100
75
50
37
25
D
30
60
90
120
150
180
(min)
E
Before bleach
After bleach
0
50
100
150
200
250 (s)
Normalised fluorescence intensity
1.4
1.2
1
0.8
0.6
0.4
0.2
0
-0.2
-50
0
50
100
150
200
250
Time (s)

[Fig. 7]

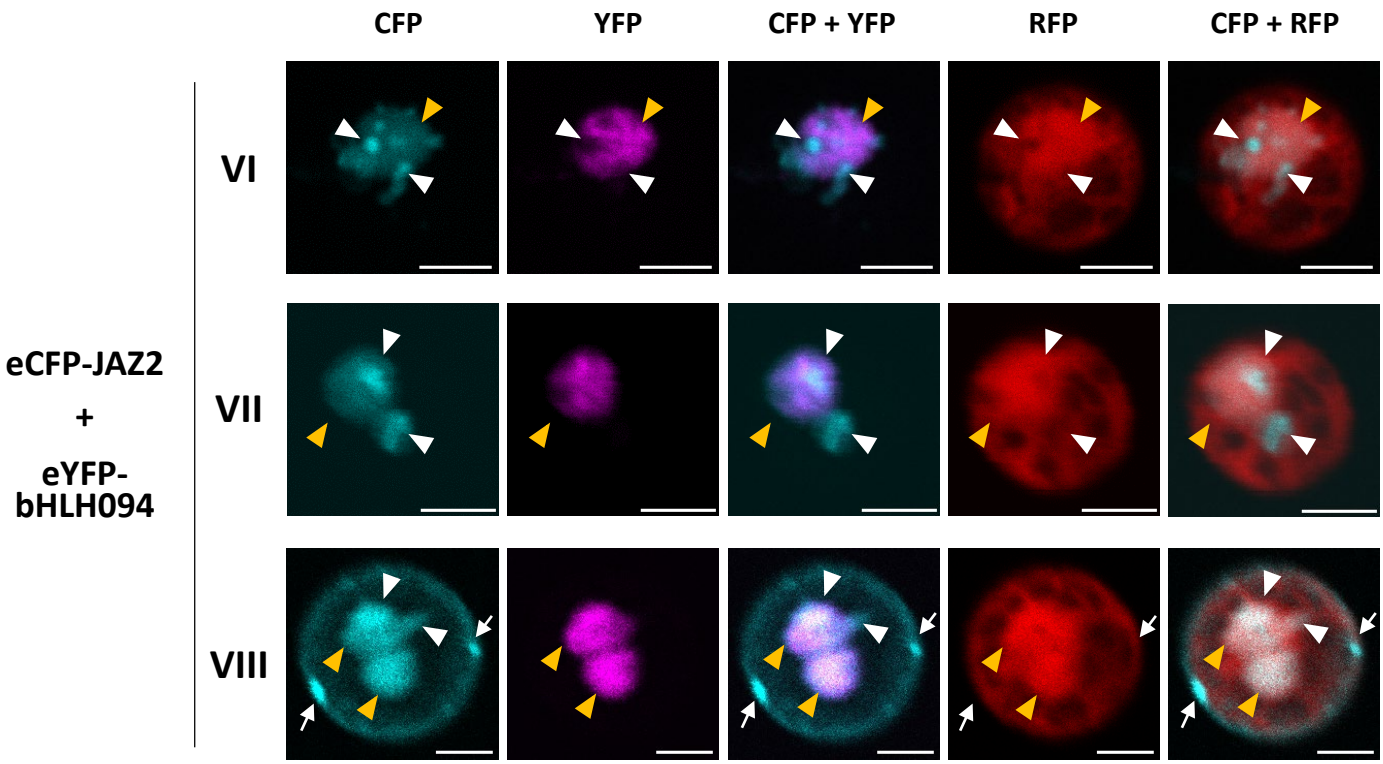

Supplementary Fig. 1 Various JAZ2 condensate patterns in *Oryza sativa* protoplasts. Fluorescence microscopy of *O. sativa* protoplasts expressing eCFP–JAZ2, eYFP–bHLH094, and mRFP1; CFP, YFP, and RFP images are shown with pseudo-colours. (VI–VIII) Subcellular localisation patterns of eCFP–JAZ2 with JAZ2 foci in three more representative cells in addition to those in **Fig. 1**. The position of JAZ2 condensates and nucleus are indicated with white and orange arrowheads or arrows, respectively. VI, several JAZ2 condensates in the nucleus and the vicinity of the nucleus are observed. VII, large JAZ2 condensates in the vicinity of the nucleus are observed. VIII, JAZ2 condensates are present in the vicinity of the nucleus (white arrowheads), as well as near the plasma membrane (white arrows) in the cytosol. Scale bars, 5 μm. eYFP–bHLH094 and mRFP1 were expressed for visualisation of the nucleus (YFP) and both the nucleus and cytosol (RFP), respectively. The position of some JAZ2 foci is devoid of YFP and/or RFP signals

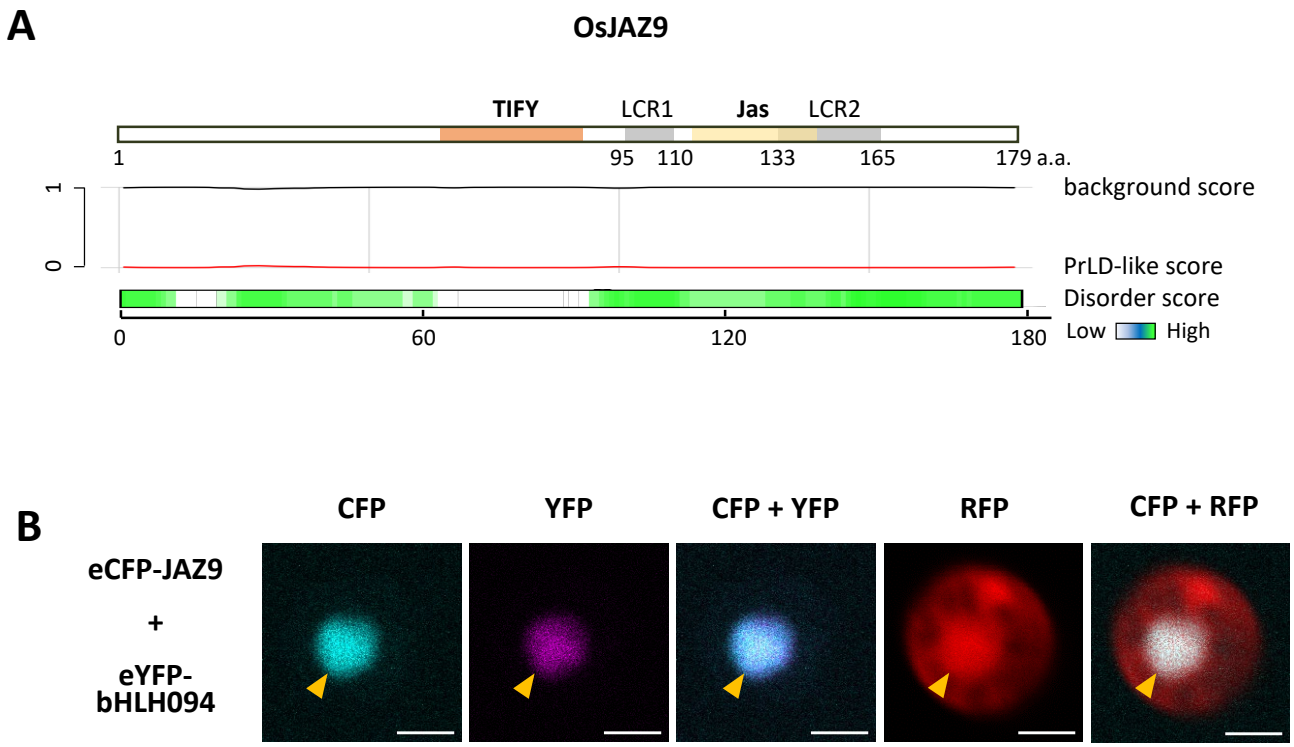

Supplementary Fig. 2 OsJAZ9 does not form condensates in *Oryza sativa* protoplasts. **(A)** Top, schematic domain structure of OsJAZ9. TIFY and Jas domains and two low-complexity regions (LCRs) are depicted. The amino acid sequences of LCR2 and Jas domain partially overlap. Bottom, Prion-like domain (PrLD) and disordered regions predicted by 'Prion-like Amino Acid Composition' (PLAAC; http://plaac.wi.mit.edu/) and 'Database of Disordered Protein Prediction' (D^2P^2; https://d2p2.pro/) algorithms, respectively. **(B)** Fluorescence microscopy of *O. sativa* protoplasts expressing eCFP–JAZ9, eYFP–bHLH094, and mRFP1. CFP, YFP, and RFP images are shown with pseudo-colours. No JAZ9 condensate, but nuclear localisation of JAZ9, is observed. eYFP–bHLH094 and mRFP1 were expressed for visualisation of the nucleus (YFP) and both the nucleus and cytosol (RFP), respectively. The position of the nucleus is indicated by orange arrowheads. Scale bars, 5 μm

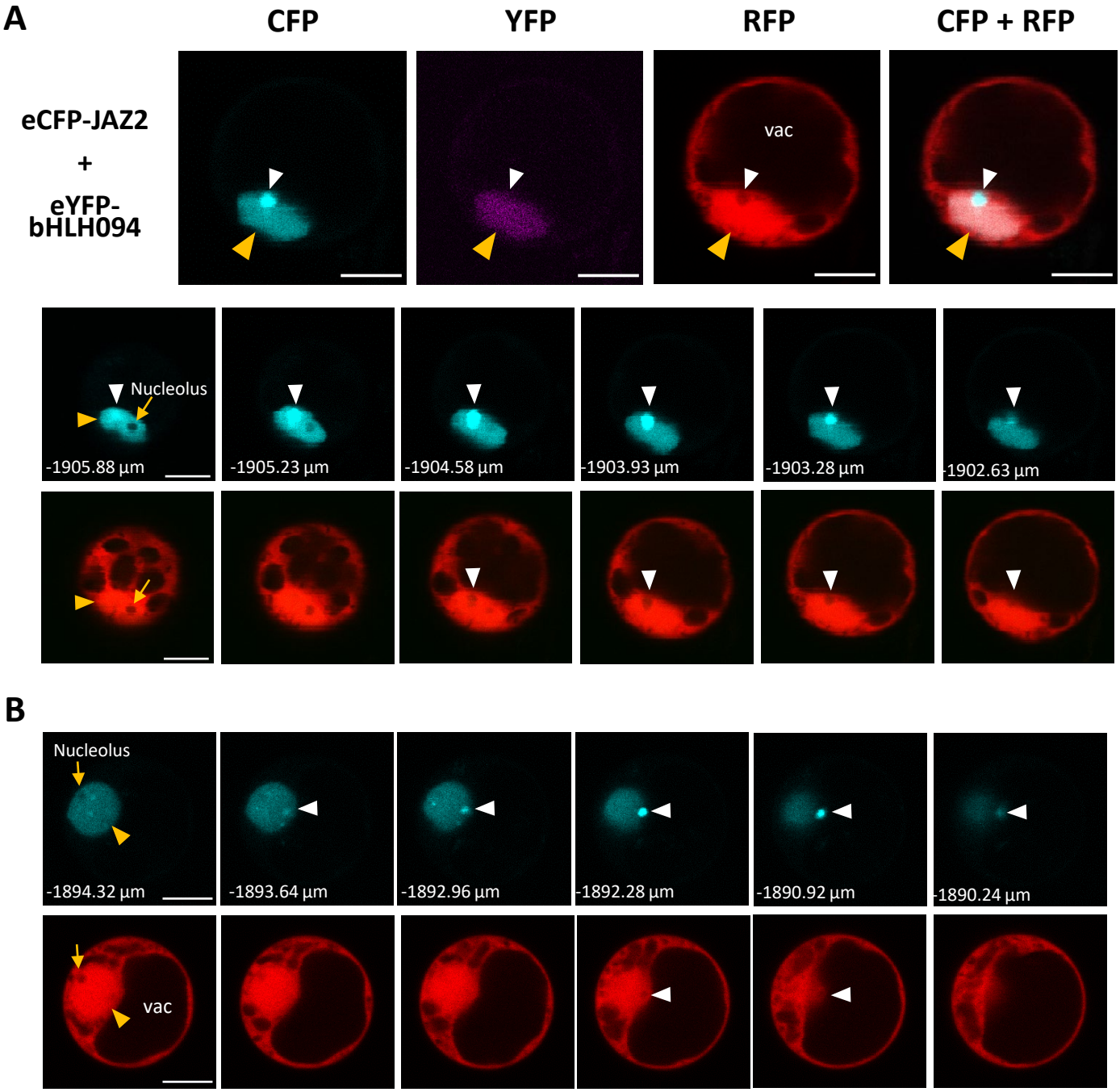

Supplementary Fig. 3 JAZ2 condensates form subcellular compartments in *Oryza sativa* protoplasts. (A) Fluorescence microscopy of a *O. sativa* protoplast expressing eCFP–JAZ2, eYFP–bHLH094, and mRFP1. Top, CFP, YFP, and RFP images are shown with pseudo-colours. eYFP–bHLH094 and mRFP1 were expressed for visualisation of the nucleus (YFP) and both the nucleus and cytosol (RFP), respectively. The positions of JAZ2 condensates and the nucleus are indicated by white and orange arrowheads, respectively. RFP fluorescence is less visible at the position of the JAZ2 condensate observed with CFP fluorescence. Bottom, Z-stack image sets of CFP (upper panels) and RFP (lower panels) of the same cell are shown in the top panels. **(B)** Z-stack image sets of CFP (upper panels) and RFP (lower panels) of the cell shown in **Figs. 1B** (panel II) and **1C**. RFP fluorescence is less visible at the JAZ2 condensate position observed with CFP fluorescence, most likely in the vicinity of the nucleus. All images in this figure were obtained with an 100× objective lens. Vac, vacuole. Scale bars, 5 µm

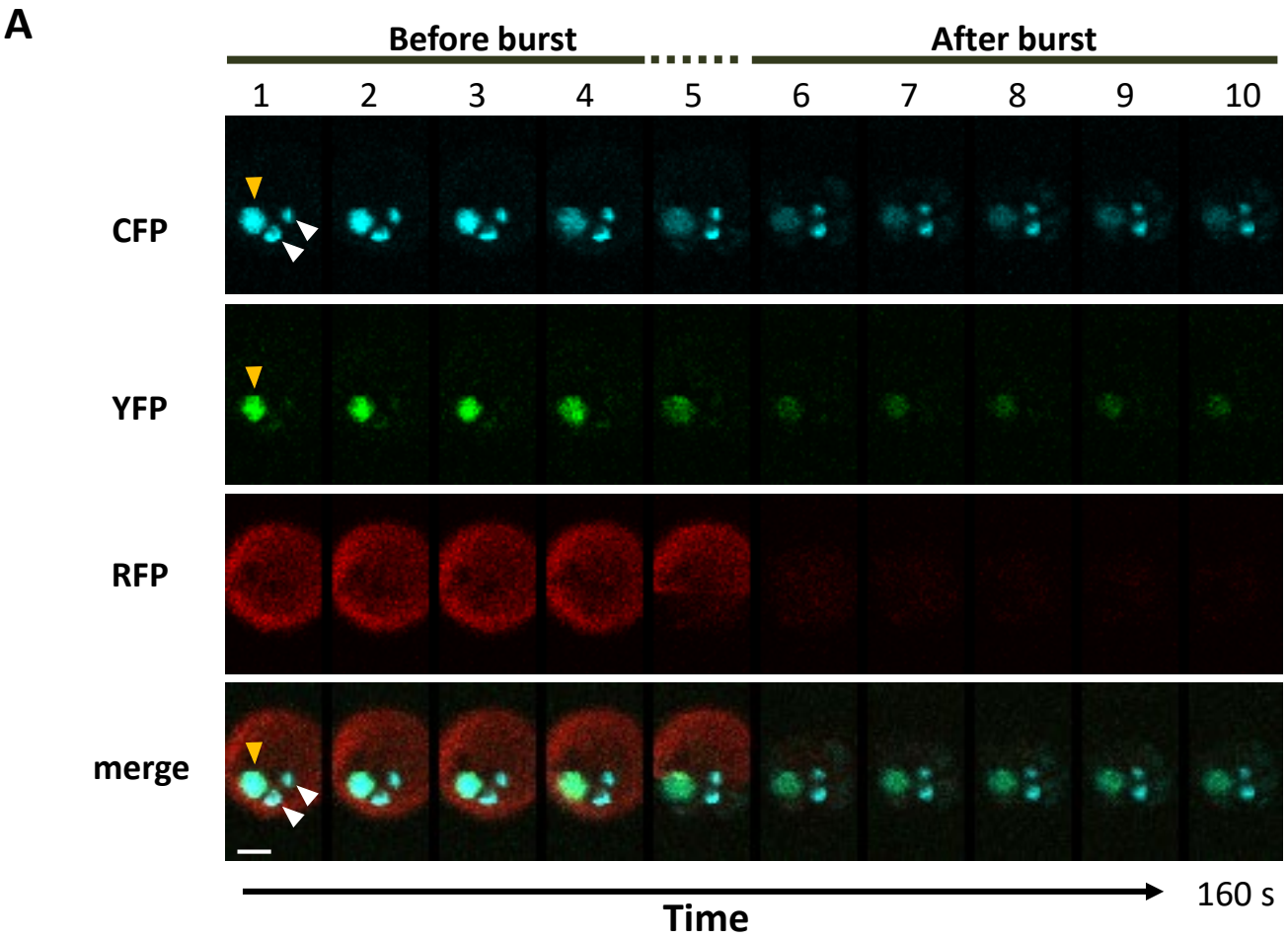

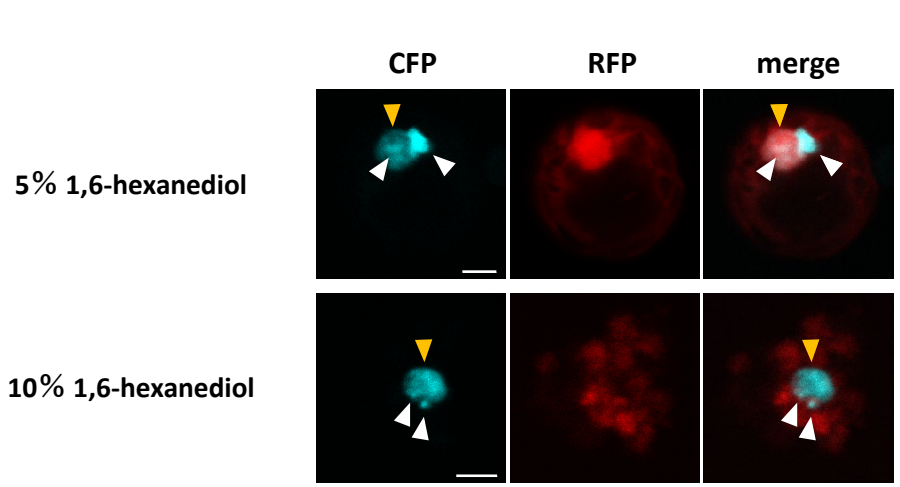

Supplementary Fig. 4 JAZ2 condensates are stable after protoplast burst and 1,6-hexanediol (HD) treatment. (A) Time-lapse images of a protoplast before and after the burst. An *Oryza sativa* protoplast expressing eCFP–JAZ2, eYFP–bHLH094, and mRFP1 burst in a hypotonic solution by diluting the protoplast suspension with an equal volume of water and reducing the osmotic pressure. The images were obtained every 16 s. The CFP, YFP, and RFP images are shown in pseudo-colours. The JAZ2 condensate positions in the cytosol and nucleus are indicated by white and orange arrowheads, respectively. A protoplast burst was observed during scanning the fifth image. CFP foci in the cytosol were visible even after the RFP markers were diffused in the sixth–tenth images. Scale bar, 5 µm **(B)** Effect of 1,6-HD on the stability of eCFP-JAZ2 condensates *in vivo*. *O. sativa* protoplasts expressing eCFP-JAZ2, eYFP–bHLH094, and mRFP1 were treated with 5% 1,6-HD for 30 min, or 10% 1,6-HD for 5 min. Protoplast structure was disrupted by 10% 1,6-HD as observed with the RFP image. Scale bar, 5 µm. Note that, after 5% and 10% 1,6-HD treatments, it took 5 and 20 minutes for observation, respectively

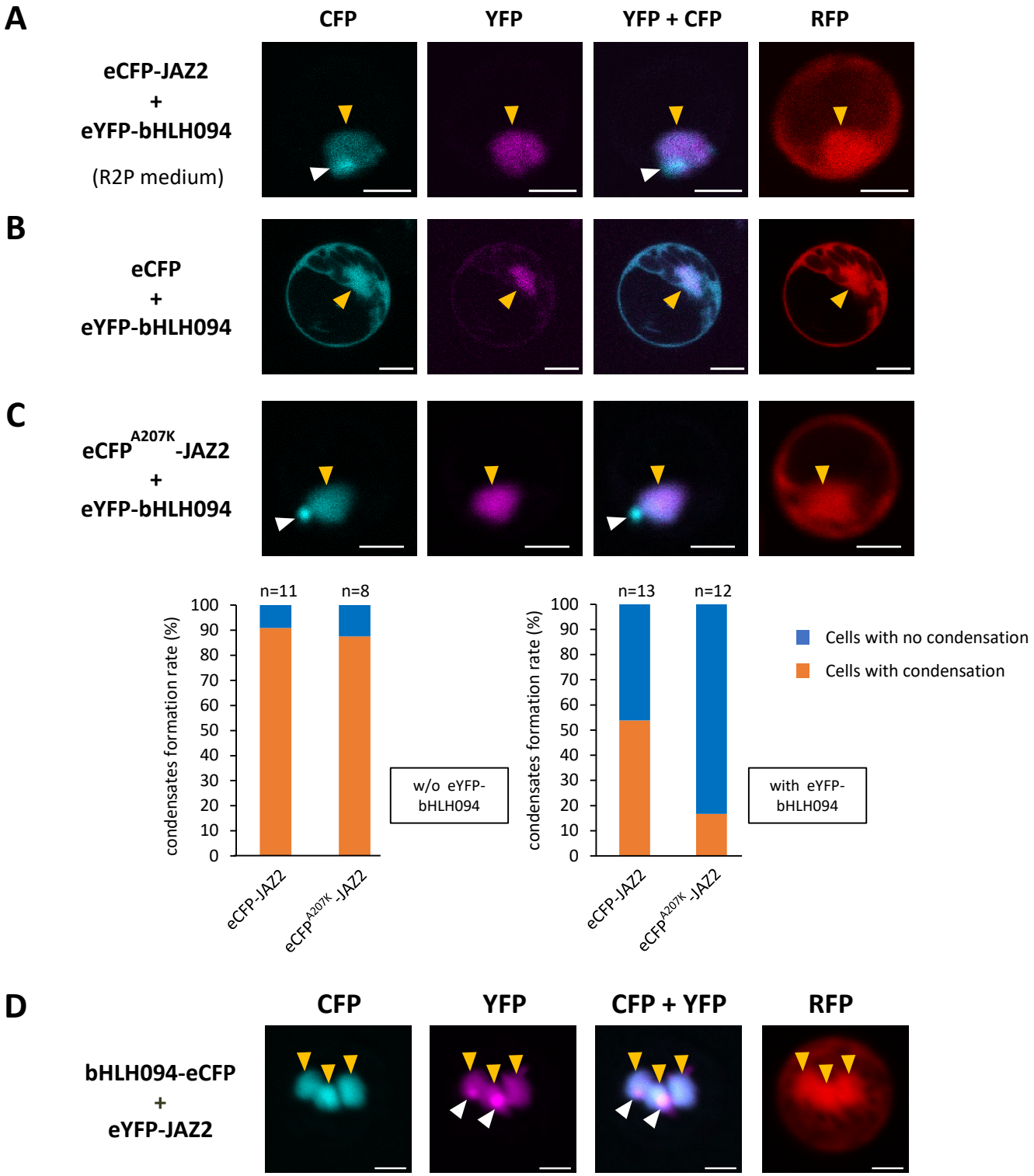

Supplementary Fig. 5 JAZ2 condensates in a rich medium, without a CFP dimerisation site, and by fusion with eYFP instead of eCFP. **(A)** JAZ2 condensate formed in *Oryza sativa* protoplasts expressing eCFP–JAZ2, eYFP–bHLH094, and mRFP1 cultured in R2P medium. **(B)** *O. sativa* protoplast expressing eCFP, eYFP–bHLH094, and mRFP1. CFP and RFP fluorescence patterns were almost similar, and no CFP foci showing condensation were observed. **(C)** Top, *O. sativa* protoplast expressing eCFP–JAZ2$^{\mathbf{A207K}}$, eYFP–bHLH094, and mRFP1. Bottom, eCFP–JAZ2 and eCFP–JAZ2$^{\mathbf{A207K}}$ condensation formation rate in the absence (left graph) or presence (right graph) of co-expressed eYFP–bHLH094. **(D)** An *O. sativa* protoplast expressing eYFP-fused JAZ2 with bHLH094–eCFP and mRFP1. The JAZ2 condensate and nucleus positions are indicated by white and orange arrowheads, respectively. The images in (B) were obtained using an 100× objective lens. In (D), three nuclei were observed in the cell, likely because of cell fusion. Scale bar, 5 μm

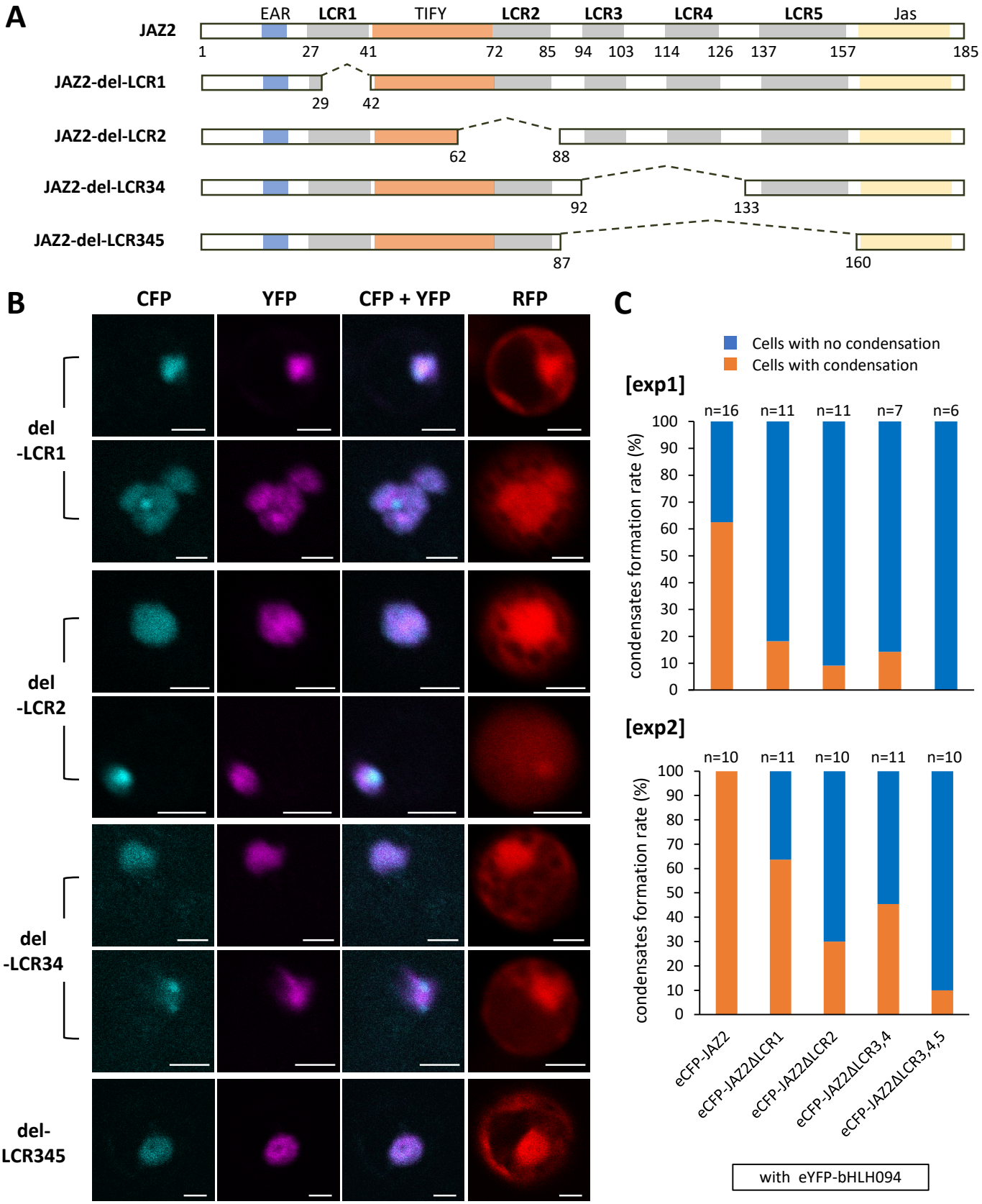

Supplementary Fig. 6 LCR deletion compromises JAZ2 condensation. **(A)** JAZ2 constructs used for deletion analysis. TIFY and Jas domains, EAR motif, and low-complexity regions (LCRs) are depicted as in **Fig. 1A**. The position of amino acid is indicated. **(B)** Fluorescence images of *Oryza sativa* protoplasts expressing eCFP-fused JAZ2 and its deletion variants with eYFP–bHLH094 and mRFP1. Representative images (top) without and (bottom) with obvious JAZ2 condensates for each deletion construct except del-LCR345. **(C)** JAZ2 condensate formation frequency. The rate of cells with and without obvious JAZ2 condensate formation by eCFP-fused construct expression in (A) with eYFP–bHLH94 in *O. sativa* protoplasts are shown. The number of JAZ2–del-LCR34 and JAZ2–del-LCR345 cells with CFP fluorescence was relatively low

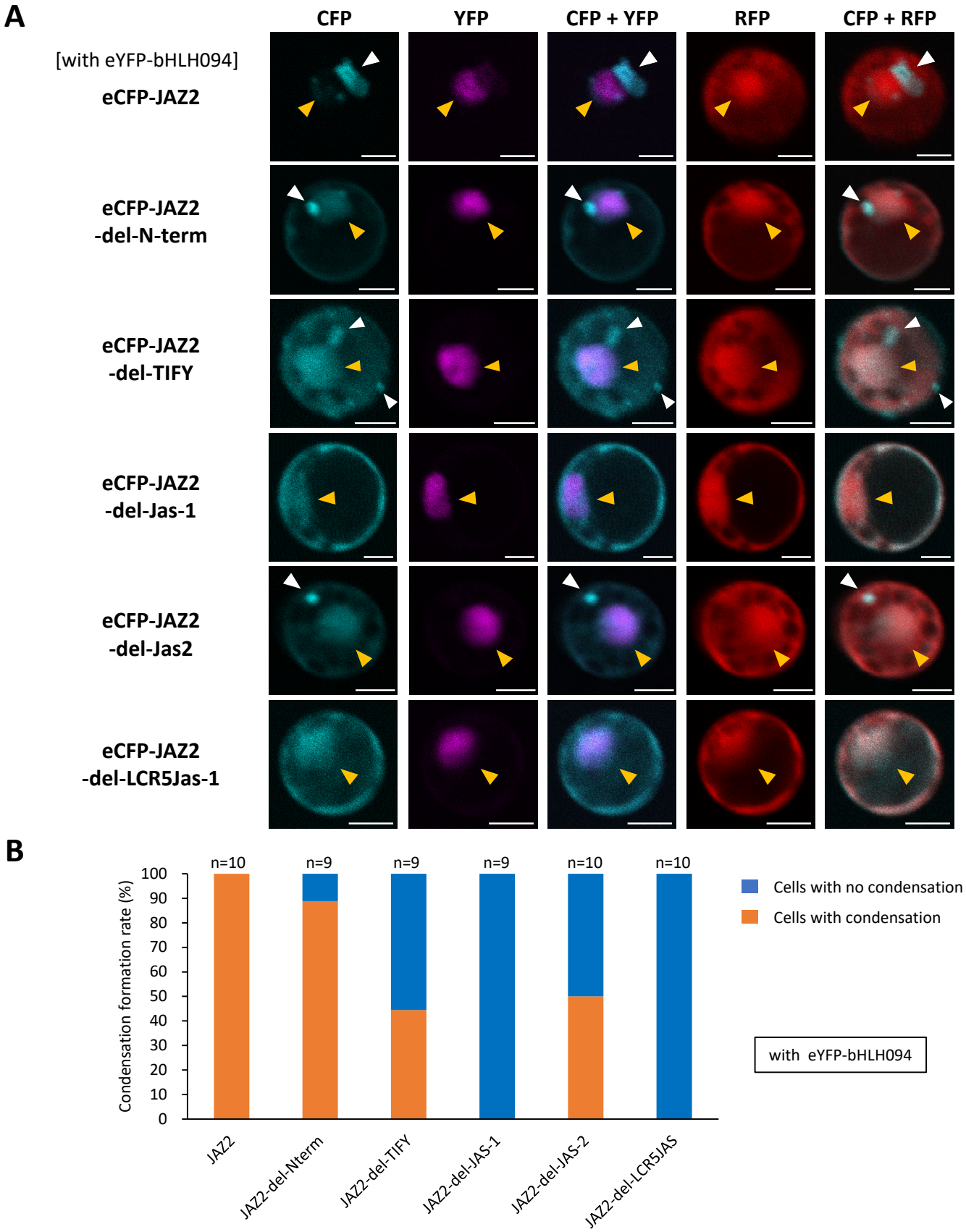

Supplementary Fig. 7 TIFY and Jas domains are involved in stable JAZ2 condensate formation. **(A)** Typical patterns of JAZ2 condensates formed in *Oryza sativa* protoplasts expressing eCFP-fused JAZ2 and its variants containing various deletions, as shown in **Fig. 3**, with eYFP–bHLH094 and mRFP1. JAZ2 condensate and nucleus positions are indicated by white and orange arrowheads, respectively. Scale bars, 5 μm. **(B)** JAZ2 condensate formation frequency. Rate of cells with and without obvious JAZ2 condensate formation by expression of eCFP-fused constructs indicated in (A) and **Fig. 3** with eYFP–bHLH094 in *O. sativa* protoplasts. The number of cells observed is indicated in the graph. Similar results were obtained by an independent experiment as shown in **Fig. 3**

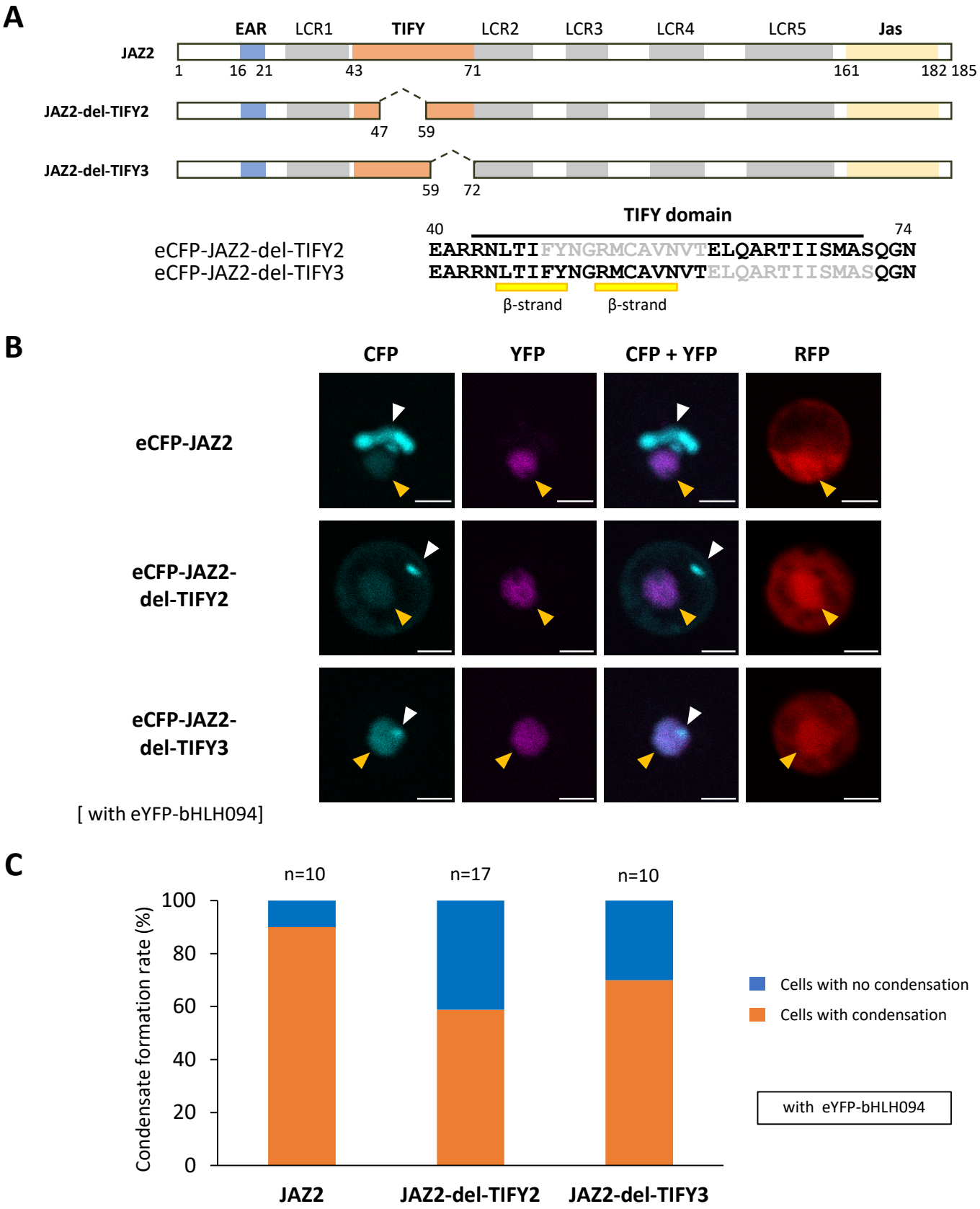

Supplementary Fig. 8 TIFY domain is involved in eCFP–JAZ2 condensate formation. (A) JAZ2 constructs used for deletion analysis. TIFY and Jas domains, EAR motif, and low-complexity regions (LCRs) are depicted as in **Fig. 1A**. The position of amino acid is indicated. Yellow bars depict the sequence predicted to form a β-strand (see also **Supplementary Fig. 10**). **(B)** Typical fluorescence images of JAZ2 condensates in *Oryza sativa* protoplasts expressing eCFP–JAZ2 and its deletion variants with eYFP–bHLH094 and mRFP1. The positions of JAZ2 condensates and the nucleus are indicated by white and orange arrowheads. Scale bar, 5 μm**. (C)** Frequency of JAZ2 condensate formation. The rate of cells with and without obvious JAZ2 condensate formation by expression of eCFP-fused constructs indicated in (A) with eYFP–bHLH094 and mRFP1 in *O. sativa* protoplasts is shown

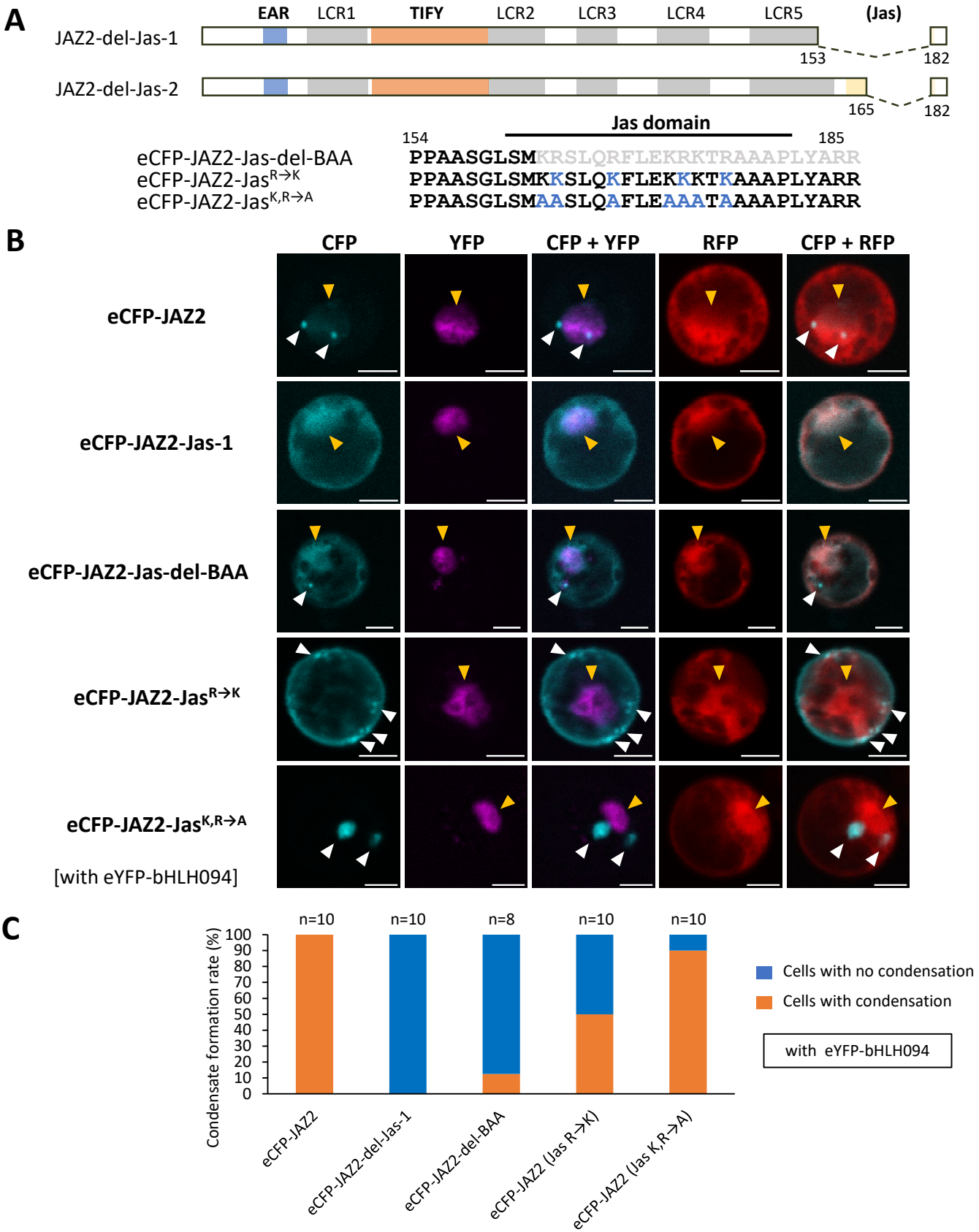

Supplementary Fig. 9 Mutations in Jas domain affect condensate formation of eCFP-JAZ2. (A) Constructs of JAZ2 with mutations in the Jas domain. TIFY and Jas domains, EAR motif, and low-complexity regions (LCRs) are depicted as in **Fig. 1A**. The position of amino acid is indicated. Grey and blue letters indicate deletion and substitution of amino acids, respectively. **(B)** Typical fluorescence images of JAZ2 condensates in *Oryza sativa* protoplasts expressing eCFP–JAZ2 and its deletion variants with eYFP–bHLH094 and mRFP1. The positions of JAZ2 condensates and the nucleus are indicated by white and orange arrowheads. **(C)** JAZ2 condensate formation frequency. The rate of cells with and without obvious JAZ2 condensate formation by expression of eCFP-fused constructs indicated in (A) with eYFP–bHLH094 and mRFP1 in *O. sativa* protoplasts is shown

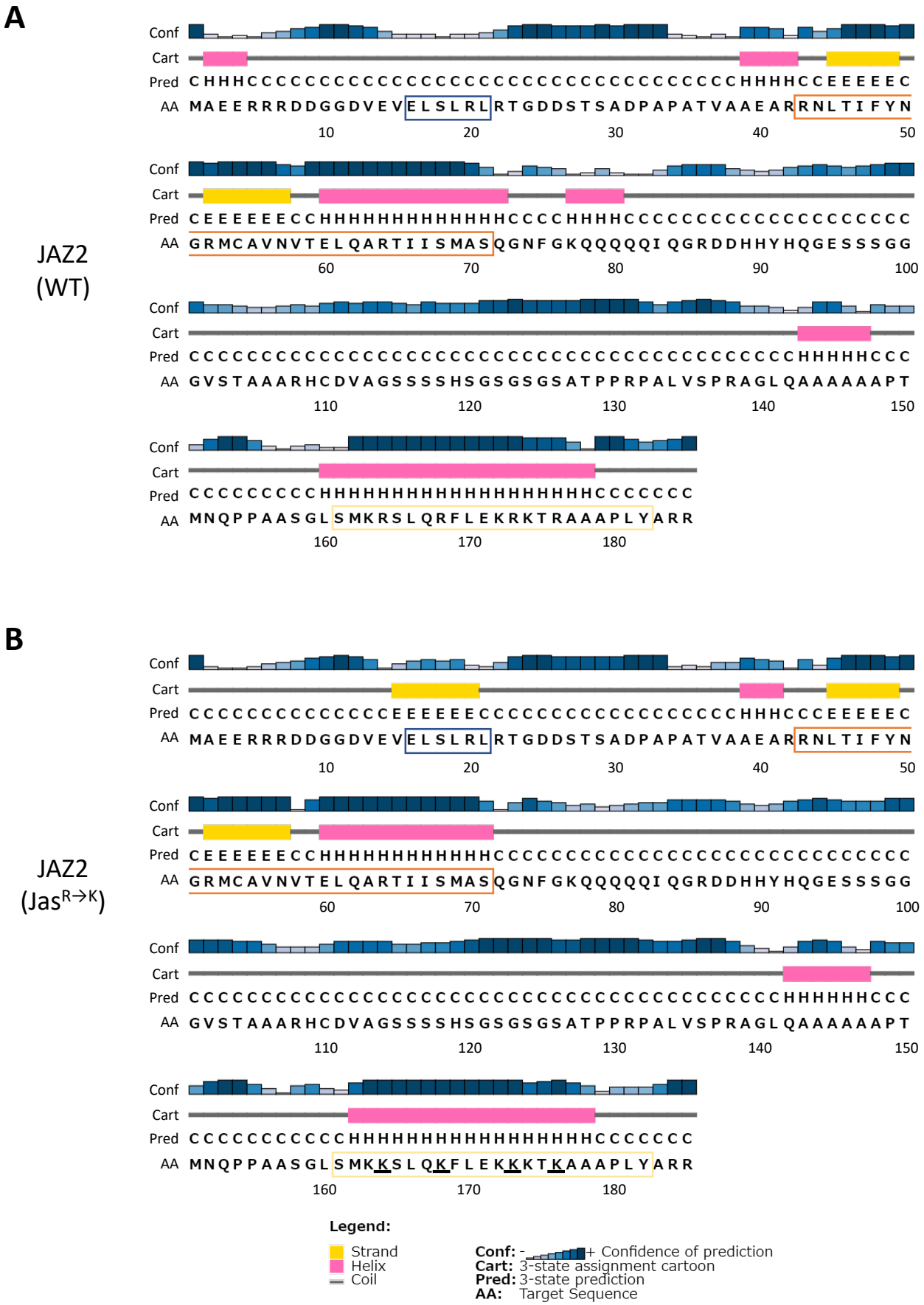

Supplementary Fig. 10 Secondary structure of (A) JAZ2 and its variates (B) JAZ2-Jas$^{R\rightarrow K}$ and (C) JAZ2-Jas$^{K,R\rightarrow A}$. Secondary structure prediction was performed using PSIPRED (http://bioinf.cs.ucl.ac.uk/psipred). The amino acid sequences of the EAR motif, the TIFY domain, and the Jas domain are shown in blue, red, and yellow, respectively. Substituted amino acids in the Jas domain are underlined in panels B and C

C

JAZ2 (Jas$^{K,R\rightarrow A}$)

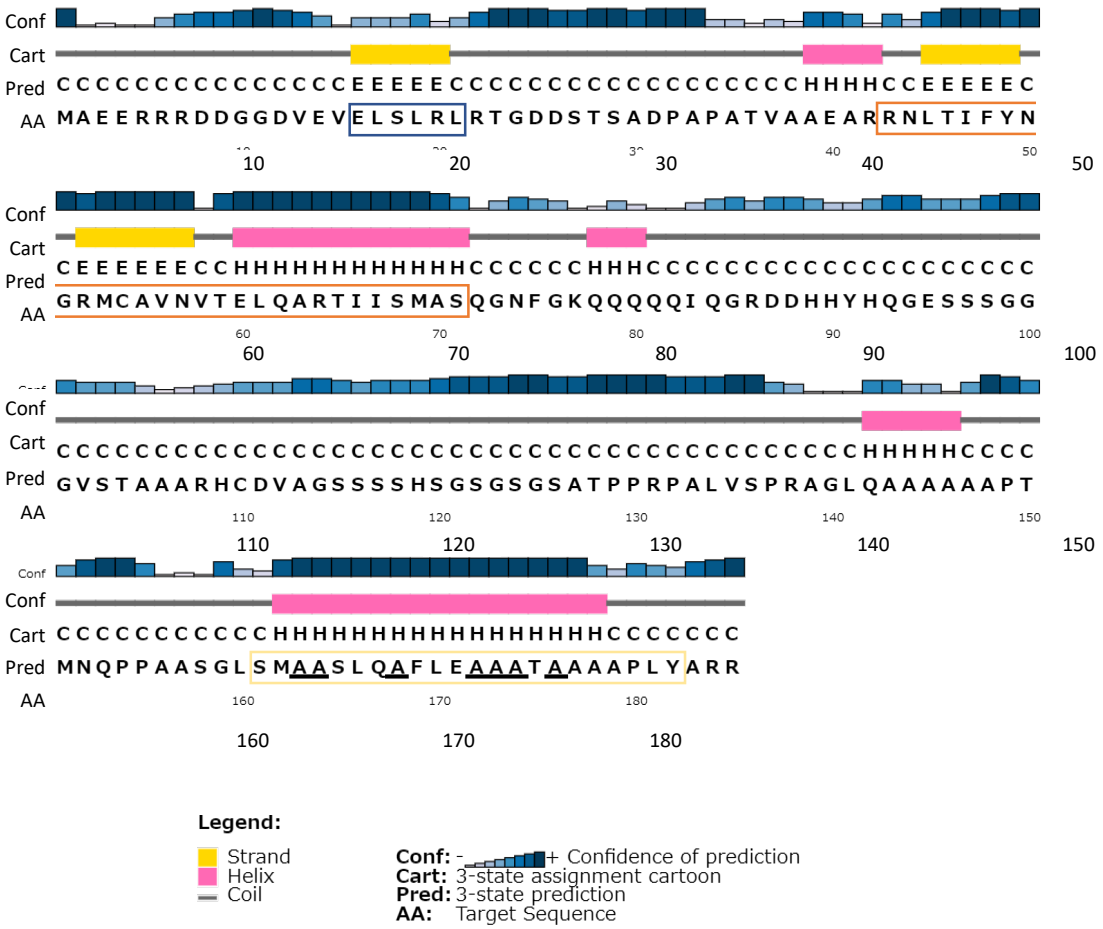

Legend:

Strand
Helix
Coil

Conf: - + Confidence of prediction
Cart: 3-state assignment cartoon
Pred: 3-state prediction
AA: Target Sequence

Supplementary Fig. 10 (continued)

Secondary structure of (A) JAZ2 and its variates (B) JAZ2-Jas$^{R\rightarrow K}$ and (C) JAZ2-Jas$^{K,R\rightarrow A}$. Secondary structure prediction was performed using PSIPRED (http://bioinf.cs.ucl.ac.uk/psipred). The amino acid sequences of the EAR motif, the TIFY domain, and the Jas domain are shown in blue, red, and yellow, respectively. Substituted amino acids in the Jas domain are underlined in panels B and C

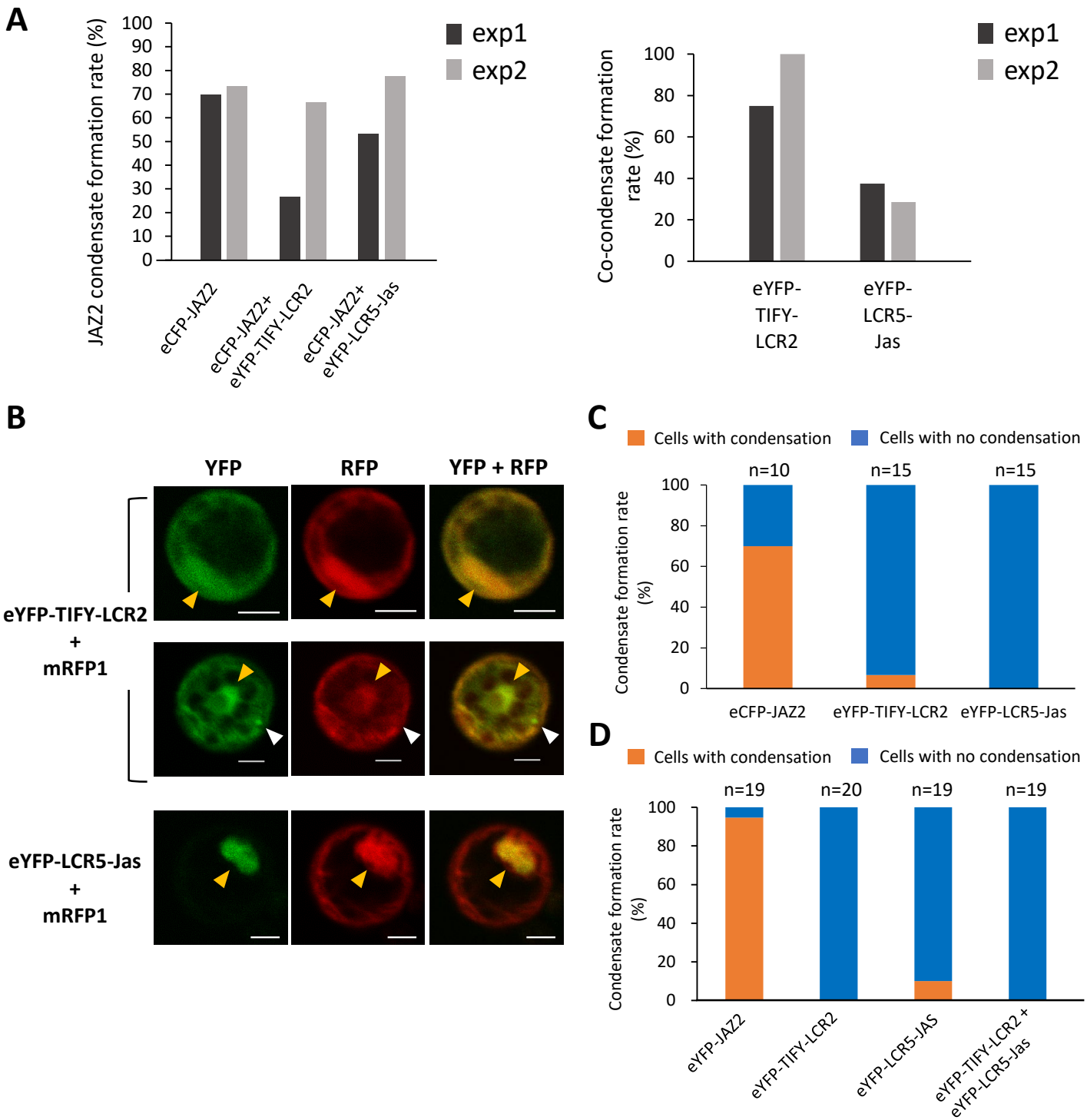

Supplementary Fig. 11 TIFY–LCR2 and LCR5–Jas can be incorporated into JAZ2 condensates. **(A)** eYFP–TIFY–LCR2 and eYFP–LCR5–Jas were co-expressed with eCFP–JAZ2 and mRFP1 in *Oryza sativa* protoplasts, as in **Fig. 4B**. Left, effects of eYFP–TIFY–LCR2 and eYFP–LCR5–Jas co-expression on JAZ2 condensation. The ratio of the cells containing JAZ2 condensates is shown. Right, the ratio of cells exhibiting YFP and CFP signal co-condensation among the cells containing eCFP–JAZ2 condensates. **(B)** eYFP–TIFY–LCR2 or eYFP–LCR5–Jas alone rarely form condensates. Fluorescence images of *O. sativa* protoplasts expressing eYFP-fused TIFY–LCR2 and LCR5–Jas with mRFP1, but without eCFP–JAZ2. The eYFP–TIFY–LCR2 condensate and nucleus positions are indicated by white and orange arrowheads, respectively. **(C)** The rate of cells with and without obvious condensate formation of the indicated fusion proteins with mRFP1 in *O. sativa* protoplasts (in the experiment indicated in B). As control, the ratio of cells with JAZ2 condensates among the cells expressing eCFP–JAZ2 with mRFP1 is shown. **(D)** The rate of cells with and without condensate formation by eYFP–JAZ2, eYFP–TIFY–LCR2, and eYFP–LCR5–Jas expression, and combinational expression of eYFP–TIFY–LCR2 and eYFP–LCR5–Jas, respectively, with mRFP1 in *O. sativa* protoplasts

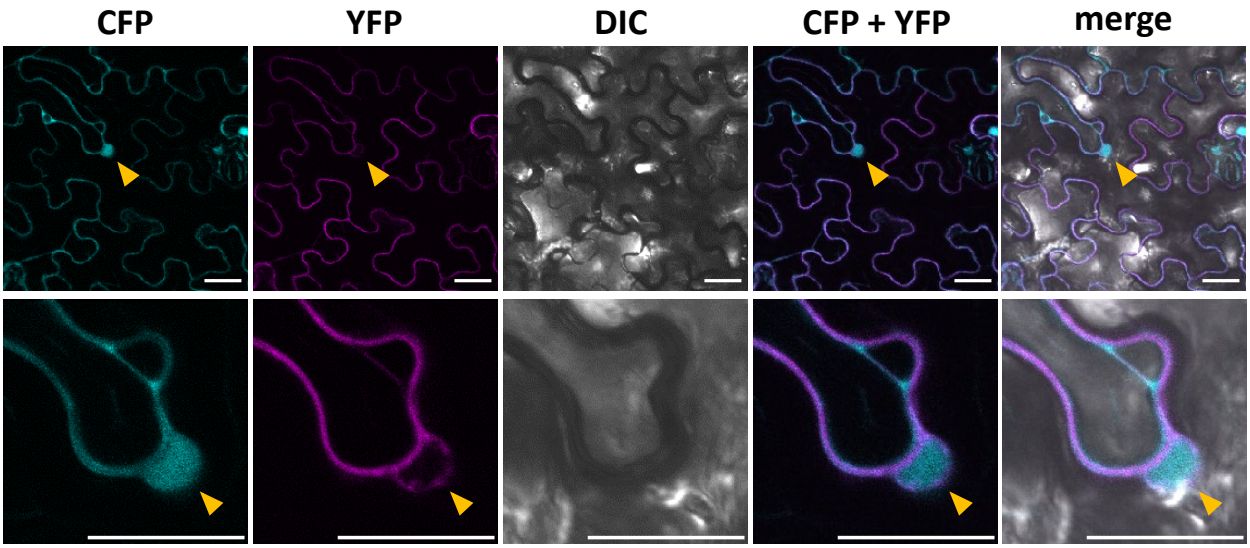

Supplementary Fig. 12 Fluorescence microscopy of *N. benthamiana* leaf epidermal cells expressing eCFP and OsSCAMP1$^{\Delta N118}$-eYFP. The CFP and YFP images are shown in pseudo-colours, with differential interference contrast (DIC) and merged images. Magnified views of the nucleus and its vicinity are shown beneath the respective cell panels. The nuclei positions are indicated by arrowheads. A truncated version of a transmembrane OsSCAMP1 protein (*Oryza sativa* secretory carrier membrane protein, OsSCAMP$^{\Delta N118}$, was fused to eYFP and co-expressed as a marker to visualise the plasma membrane and internal membranes, as OsSCAMP1 localises to the plasma membrane and trans-Golgi network or early endosomes (Cai et al. 2011, 2012). eCFP was detected in both the nucleus (orange arrowheads) and cytosol. In contrast to eCFP–JAZ2 (**Fig. 5**), eCFP alone did not form condensates in the nucleus or its vicinity, although an association between CFP signals and some cellular components was observed. OsSCAMP1$^{\Delta N118}$–eYFP fluorescence on the plasma membrane and outside edge of the nucleus were high and low, respectively. Scale bar, 30 μm

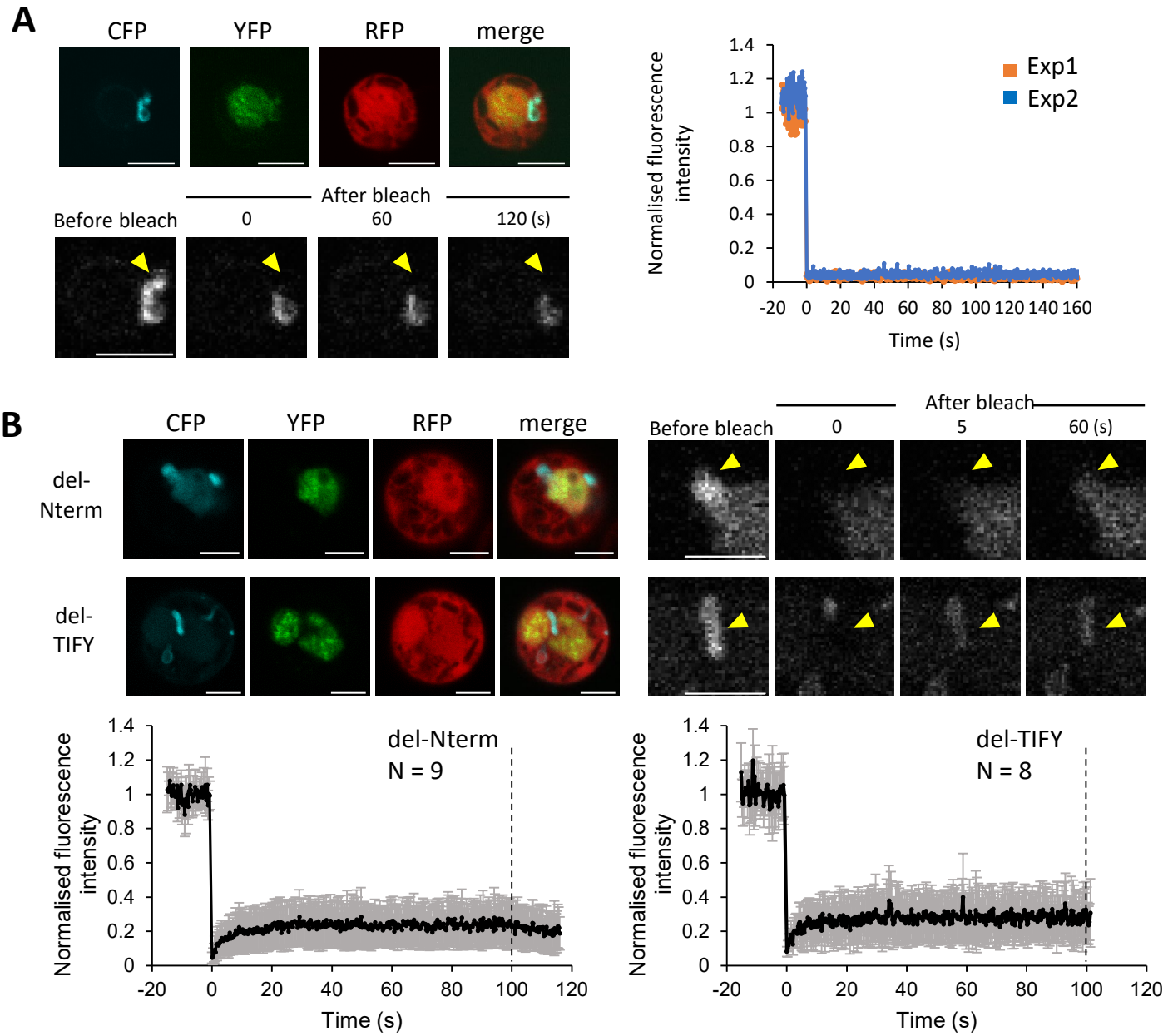

Supplementary Fig. 13 Fluorescence recovery after photobleaching (FRAP) of condensates formed by eCFP–JAZ2 and its variants. **(A)** FRAP of eCFP–JAZ2 condensates after partial bleaching, showing no fluorescence recovery. Left (top), representative fluorescence images of an *Oryza sativa* protoplast expressing eCFP–JAZ2 with eYFP–bHLH094 and mRFP1. Left (bottom), fluorescence recovery of eCFP–JAZ2 after photobleaching at the indicated position by yellow arrowheads. Time 0 indicates the time point of the bleaching pulse. Scale bar, 5 μm. Right, the normalised FRAP intensity is shown. **(B)** FRAP of condensates formed by eCFP–JAZ2ΔNterm and eCFP-JAZ2ΔTIFY, showing moderate fluorescence recovery. Top (left), representative fluorescence images of *O. sativa* protoplasts expressing eCFP–JAZ2ΔNterm and eCFP–JAZ2ΔTIFY, with eYFP–bHLH094 and mRFP1. Top (right), fluorescence recovery of condensates formed by eCFP–JAZ2ΔNterm and eCFP–JAZ2ΔTIFY, after bleaching at the indicated position by yellow arrowheads. Time 0 indicates the time point of the bleaching pulse. Scale bar, 5 μm. (Bottom), normalised FRAP intensity of the condensates, corresponding to the results shown in **Fig. 6F**

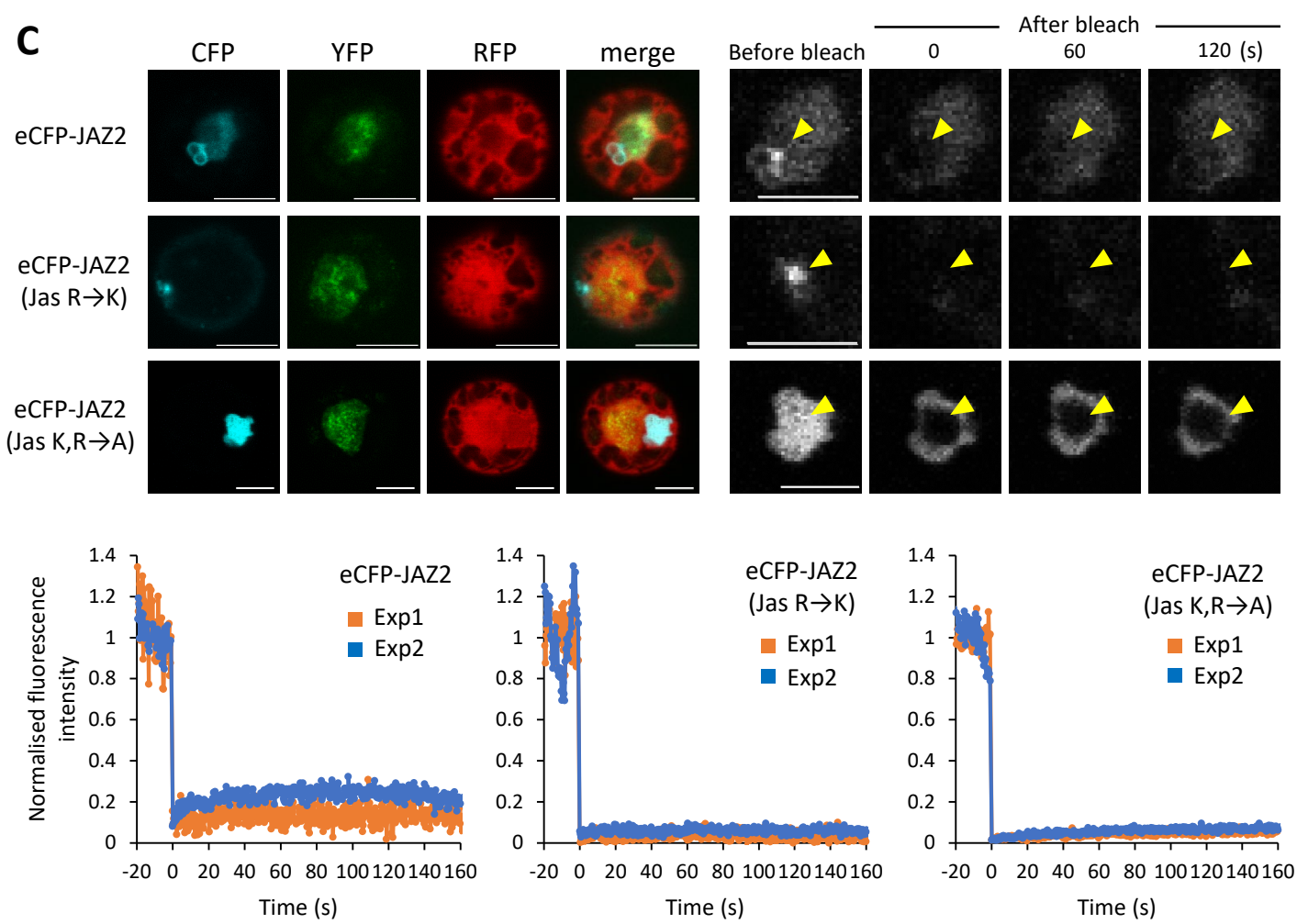

Supplementary Fig. 13 (continued)

Fluorescence recovery after photobleaching (FRAP) of condensates formed by eCFP–JAZ2 and its variants.

(C) FRAP of condensates formed by eCFP–JAZ2 and its variants. Top (left), representative fluorescence images of an *O. sativa* protoplast expressing eCFP–JAZ2 and its variants, with eYFP–bHLH094 and mRFP1. Top (right), fluorescence recovery of condensates formed by eCFP–JAZ2 and its variants, respectively, after photobleaching at the indicated position by yellow arrowheads. Time 0 indicates the time point of the bleaching pulse. Scale bar, 5 μm. (Bottom), normalised FRAP intensity

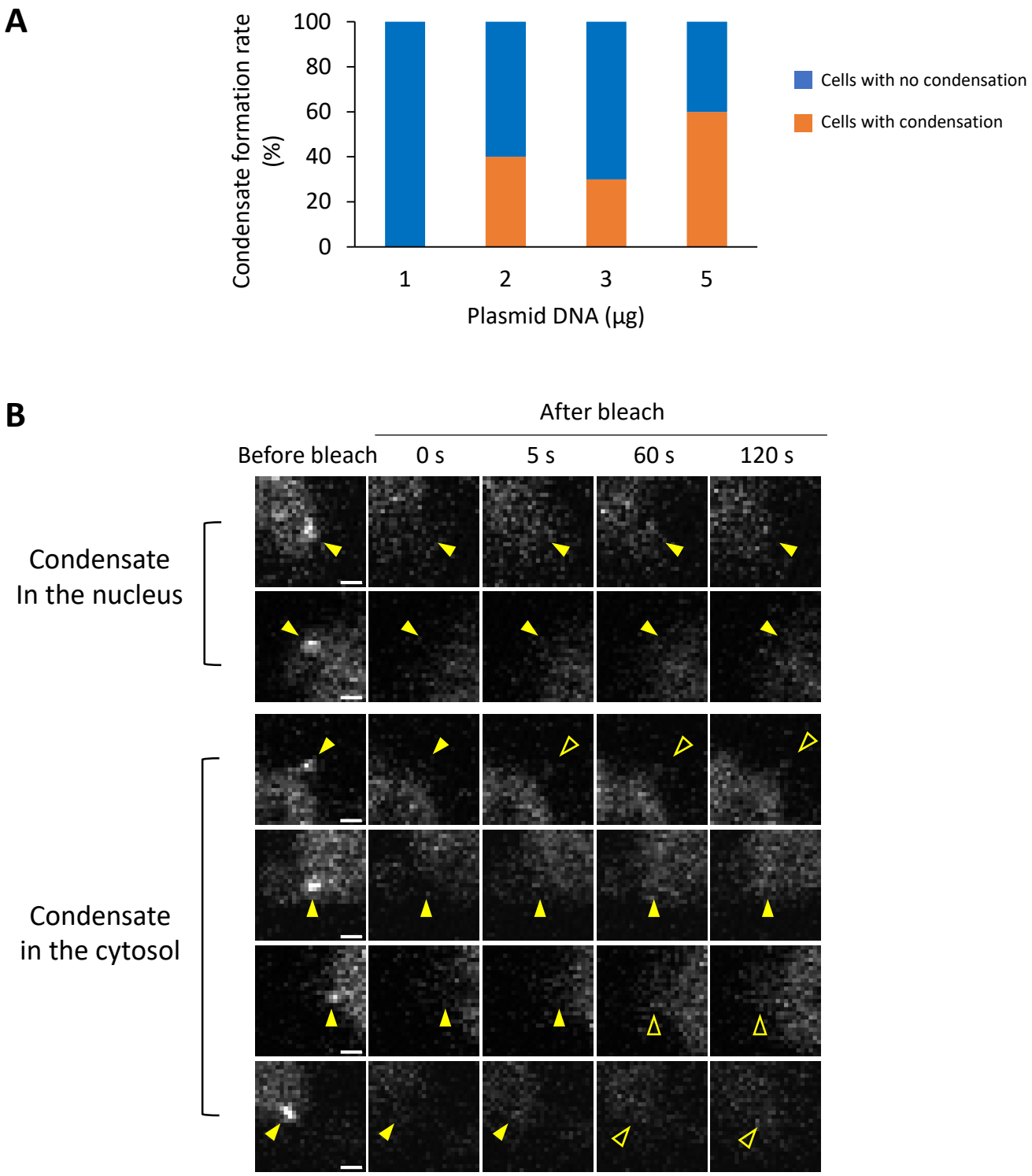

Supplementary Fig. 14 FRAP of eCFP–JAZ2 condensates in *Oryza sativa* protoplasts transfected with lower amounts of DNA. **(A)** eCFP–JAZ2 condensate formation frequency depending on the amount of plasmid DNA introduced. The indicated amount of plasmid DNA was used for the expression of eCFP–JAZ2 (see Methods for detail). Rate of cells with and without obvious JAZ2 condensate formation by expression of eCFP–JAZ2 with eYFP–bHLH094 and mRFP1 in *O. sativa* protoplasts is shown (n = 10, for each). **(B)** FRAP of eCFP-JAZ2 condensates in the nucleus and cytosol in *O. sativa* protoplasts transfected with 2 μg of plasmid DNA carrying CaMV 35S promoter::eCFP–JAZ2 as described in (A). CFP images after photobleaching at the indicated position by filled yellow arrowheads are shown. Open yellow arrowheads indicate the putative shifted position of photobleaching due to cytoplasmic flow. Time 0 indicates the time point of the bleaching pulse. Scale bar, 1 μm

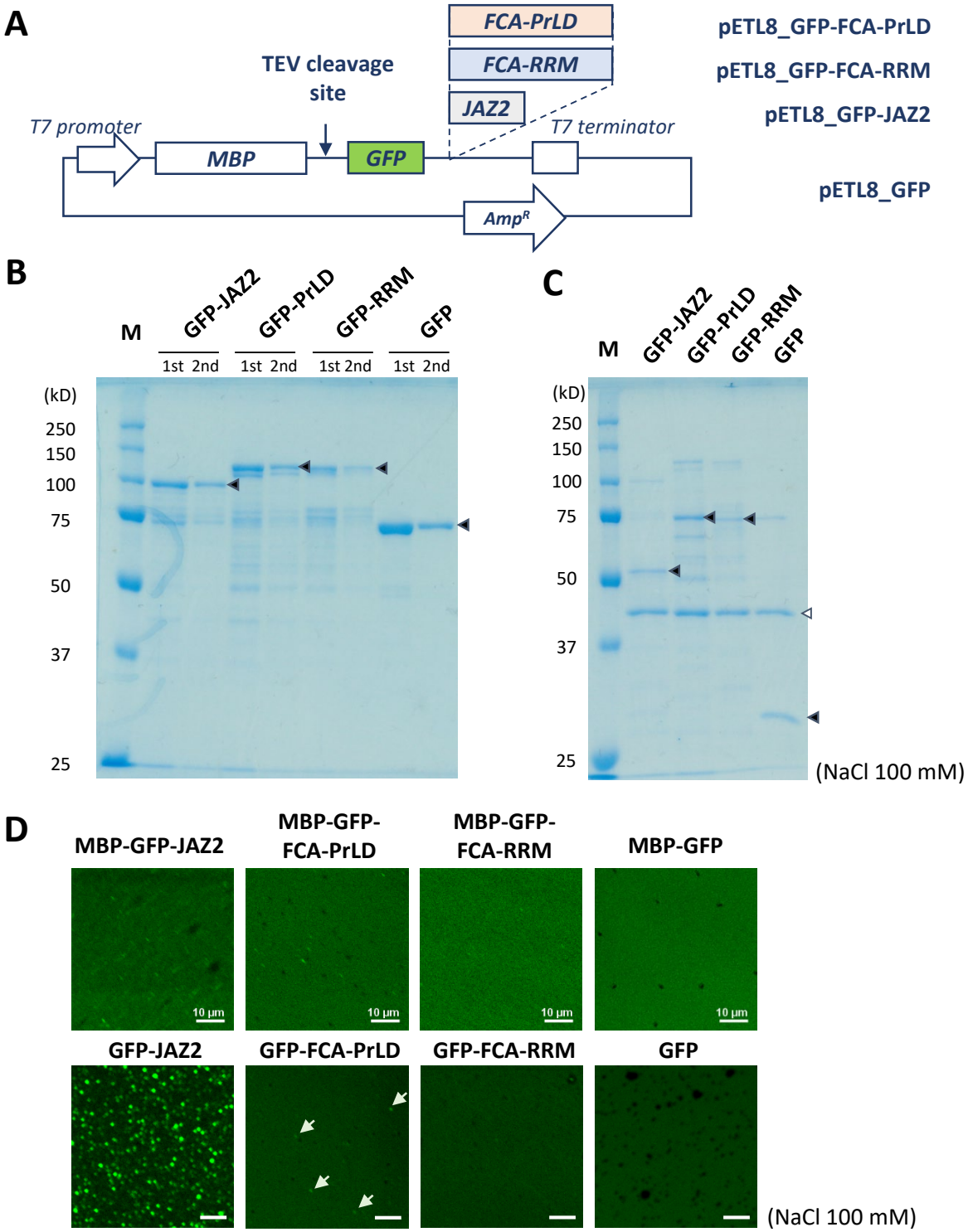

Supplementary Fig. 15 JAZ2 forms condensates *in vitro*. (A) Plasmid constructs used for protein expression in *Escherichia coli*. GFP–JAZ2, GFP–FCA–PrLD, GFP–FCA–RRM, and GFP, fused to MBP, respectively, were expressed using pETL8–GFP-derived constructs. pETL8–GFP–FCA–PrLD, pETL8–GFP–FCA–RRM, and pETL8–GFP were generous gifts from Prof. Caroline Dean of John Innes Centre. **(B)** Sodium dodecyl sulfate polyacrylamide gel electrophoresis (SDS–PAGE) of MBP-fused GFP–JAZ2, GFP–FCA–PrLD, GFP–FCA–RRM, and GFP, respectively. MBP-fused proteins (indicated by arrowheads) were eluted twice (1st and 2nd) from amylose-resign by maltose and both fractions were analysed. **(C)** SDS–PAGE of GFP–JAZ2, GFP–FCA–PrLD, GFP–FCA–RRM, and GFP (closed arrowheads), obtained after TEV protease reaction for 2 h in the presence of 100 mM NaCl. Estimated concentrations (µM) of GFP-tagged proteins after cleavage by TEV protease are 0.3 (GFP–JAZ2), 0.4 (GFP–FCA–PrLD), 0.2 (GFP–FCA–RRM) and 1.1 (GFP). Open arrowhead indicates the bands for MBP released by TEV protease reaction.

Supplementary Fig. 15 (continued)

(D) GFP fluorescence images of GFP–JAZ2, GFP–FCA–PrLD, GFP–FCA–RRM, and GFP, before (upper panels) and after (lower panels) MBP-tag removal. 1.6 times protein solutions analysed by SDS–PAGE (as in B and C) were observed using CLSM. Scale bar, 10 μm. Note that recombinant proteins were not further purified after TEV cleavage, and the protein solutions used for microscopic observation contained MBP protein and TEV protease

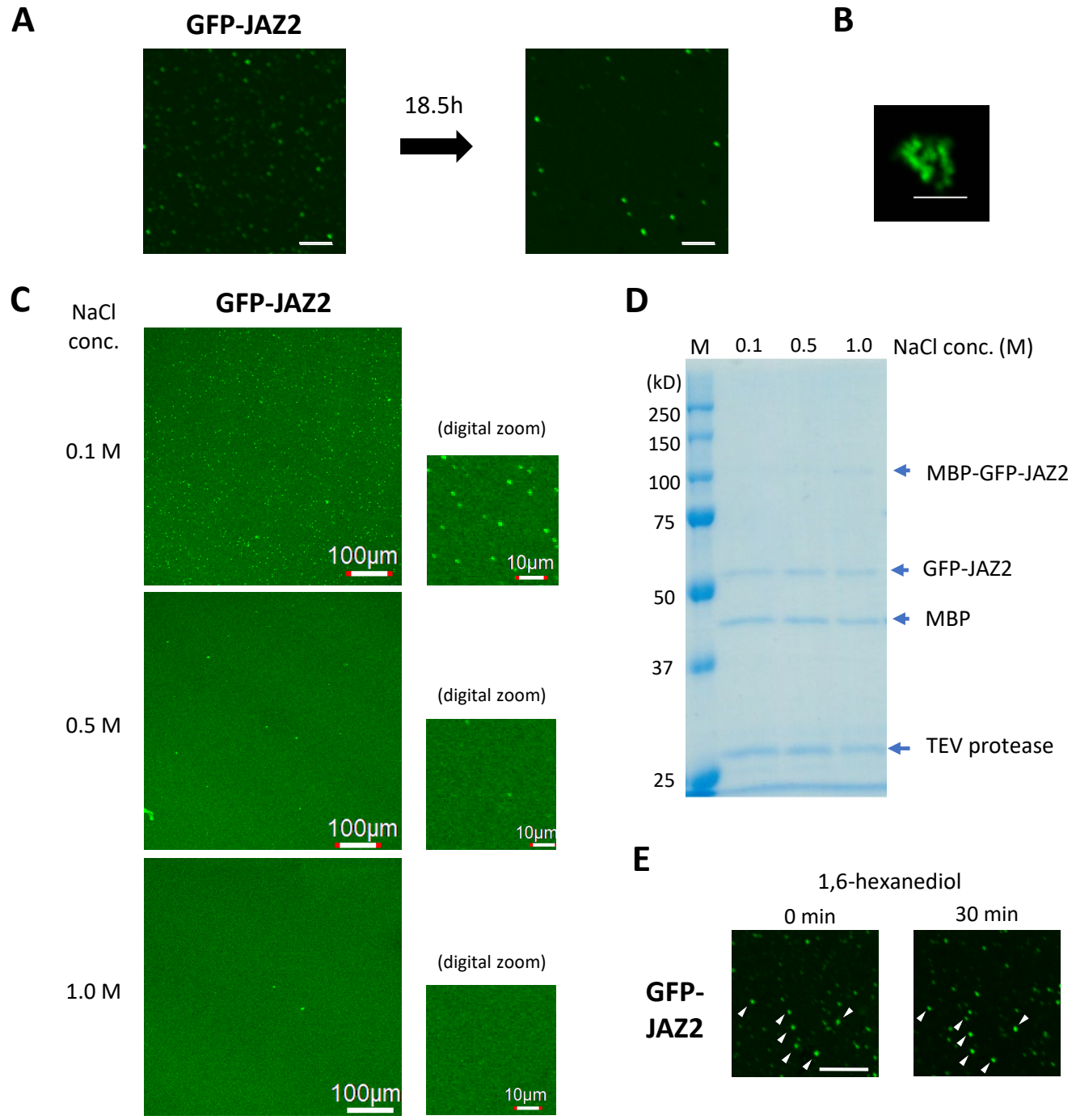

Supplementary Fig. 16 Effects of increased incubation and high salt concentration on *in vitro* JAZ2 condensate formation (A to D) and of 1,6-hexanediol (HD) on the stability of the JAZ2 condensates (E). **(A)** Size and intensity of GFP fluorescence of GFP–JAZ2 condensates were increased after an increased incubation. GFP–JAZ2 protein solution (~0.3 μM) was incubated for 18.5 h at 24 ° C after cleavage with TEV protease for 2 h in the presence of 100 mM NaCl. The increased incubation also formed non-spherical or non-ellipsoidal JAZ2 condensates. Scale bar, 10 μm. **(B)** Intricate GFP–JAZ2 condensate formed after long incubation as in (A) for 19 h at 25 ° C. Scale bar, 3 μm. **(C, D)** JAZ2 condensate formation was inhibited by high salt concentration. MBP-tagged GFP–JAZ2 was treated with TEV protease for 2 h at 30 °C in the presence of 0.1, 0.5, and 1.0 M NaCl. Resulted proteins were used for (C) GFP observation and (D) sodium dodecyl sulfate polyacrylamide gel electrophoresis (SDS–PAGE). The estimated GFP–JAZ2 concentration after cleavage by TEV protease is 0.1 μM. Note that recombinant proteins were not further purified after TEV cleavage, and the protein solutions used for microscopic observation contained MBP protein and TEV protease. **(E)** Treatment of *in vitro* JAZ2 condensates with 1,6-HD. Representative GFP–JAZ2 condensates resistant to 1,6-HD are indicated by white arrowheads. During incubation for 30 min, there are condensates newly appearing in the focal plane or deviated from the focal plane. Scale bars, 5 μm

Supplementary Table 1. Primers used for construction of plasmids

Plasmid constructs	Primer name	Sequence (5'- 3')	Template DNA	Methods used for cloning
pUGW45_eCFP-JAZ9	NotI-CACC-JAZ9-F	CTCCGCGGCCGCCCCCTTCACCATGGCGTCGACGGATCCC	pENTR_JAZ9	Restriction enzyme
	MluI-JAZ9-R	GGTCACGCGTTCAGCGCGAGTGCATGTGTCC		
pETL8-MBP-GFP-JAZ2-His-tag	BspHI-JAZ2-F	GCATTCATGATGATGGCGGAGGAGCGGAGGAG	pUGW45_eCFP-JAZ2	Restriction enzyme
	JAZ2-His-SalI-R	GCATGTCGACTTAGTGATGGTGATGGTGATGGTGATGTCGCCGGGCGTACAGCC		
pUGW45_eCFP^{A207K}, pUGW45_eCFP^{A207K}-JAZ2	sGFP-A206K-Fw	TACCTGAGCACCCAGTCCAAACTGAGCAAAGAC	pUGW45, pUGW45_eCFP-JAZ2	Site Directed Mutagenesis
	sGFP-A206K-Rv	GTCTTTGCTCAGTTTGGACTGGGTGCTCAGGTA		
pUGW45_eCFP-JAZ2-del-LCR1	JAZ2-del-LCR1-Fw	GGGGACGACAGTACAAGTAGGAGGAACTTGACCATC	pUGW45_eCFP-JAZ2	Site Directed Mutagenesis
	JAZ2-del-LCR1-Rv	GATGGTCAAGTTCCTCCTACTTGTACTGTCGTCCCC		
pUGW45_eCFP-JAZ2-del-LCR2	JAZ2-del-LCR2-Fw	AACGTCACCGAGCTACAGGATCACCACTACCACCAG	pUGW45_eCFP-JAZ2	Site Directed Mutagenesis
	JAZ2-del-LCR2-Rv	CTGGTGGTAGTGGTGATCCTGTAGCTCGGTGACGTT		
pUGW45_eCFP-JAZ2-del-LCR34	JAZ2-del-LCR34-Fw	GATCACCACTACCACCAGCTGGTTTCTCCTCGCGCG	pUGW45_eCFP-JAZ2	Site Directed Mutagenesis
	JAZ2-del-LCR34-Rv	CGCGCGAGGAGAAACCAGCTGGTGGTAGTGGTGATC		
pUGW45_eCFP-JAZ2-del-LCR345	JAZ2-del-LCR345-Fw	CAAATACAGGGTAGGGACCTGTCCATGAAGCGGTCG	pUGW45_eCFP-JAZ2	Site Directed Mutagenesis
	JAZ2-del-LCR345-Rv	CGACCGCTTCATGGACAGGTCCCTACCCTGTATTTG		
pUGW45_eCFP-JAZ2-del-Nterm	JAZ2-del-Nterm-Fw	TTCACCATGGCGGAGGAGGGGGACGACAGTACAAGT	pUGW45_eCFP-JAZ2	Site Directed Mutagenesis
	JAZ2-del-Nterm-Rv	ACTTGTACTGTCGTCCCCCTCCTCCGCCATGGTGAA		
pUGW45_eCFP-JAZ2-del-TIFY	JAZ2-del-TIFY-Fw	AGGAGGAACTTGACCATCCAAGGAAATTTCGGCAAG	pUGW45_eCFP-JAZ2	Site Directed Mutagenesis
	JAZ2-del-TIFY-Rv	CTTGCCGAAATTTCCTTGGATGGTCAAGTTCCTCCT		
pUGW45_eCFP-JAZ2-del-JAS-1	JAZ2-del-JAS-Fw1	GCGCCGACGATGAACCAGTACGCCCGGCGATAGAAG	pUGW45_eCFP-JAZ2	Site Directed Mutagenesis
	JAZ2-del-JAS-Rv1	CTTCTATCGCCGGGCGTACTGGTTCATCGTCGGCGC		
pUGW45_eCFP-JAZ2-del-JAS-2	JAZ2-del-JAS-Fw2	CTGTCCATGAAGCGGTCGTACGCCCGGCGATAGAAG	pUGW45_eCFP-JAZ2	Site Directed Mutagenesis
	JAZ2-del-JAS-Rv2	CTTCTATCGCCGGGCGTACGACCGCTTCATGGACAG		
pUGW45_eCFP-JAZ2-del-TIFY2	JAZ2-del-TIFY2-Fw	AGGAGGAACTTGACCATCGAGCTACAGGCGAGGACG	pUGW45_eCFP-JAZ2	Site Directed Mutagenesis
	JAZ2-del-TIFY2-Rv	CGTCCTCGCCTGTAGCTCGATGGTCAAGTTCCTCCT		
pUGW45_eCFP-JAZ2-del-TIFY3	JAZ2-del-TIFY3-Fw	TGCGCCGTCAACGTCACCCAAGGAAATTTCGGCAAG	pUGW45_eCFP-JAZ2	Site Directed Mutagenesis
	JAZ2-del-TIFY3-Rv	CTTGCCGAAATTTCCTTGGGTGACGTTGACGGCGCA		
pUGW45_eCFP-JAZ2-del-LCR5JAS	JAZ2-del-LCR5JAS-Fw	CTGGTTTCTCCTCGCGCGTACGCCCGGCGATAGAAG	pUGW45_eCFP-JAZ2	Site Directed Mutagenesis
	JAZ2-del-LCR5JAS-Rv	CTTCTATCGCCGGGCGTACGCGCGAGGAGAAACCAG		
pUGW45_eCFP-JAZ2-del-BAA	JAZ2-del-BAA_Fw	CGAGCGGGCTGTCCATGTACGCCCGGCGATAGAAG	pUGW45_eCFP-JAZ2	Site Directed Mutagenesis
	JAZ2-del-BAA_Rv	CTTCTATCGCCGGGCGTACATGGACAGCCCGCTCG		
pUGW45_eCFP-JAZ2-Jas$^{R\rightarrow K}$_insert	JAZ2(R toK)_insert_Fw	AAGAAGTCGCTGCAGAAGTTCCTCGAGAAGAAGAA	(primers used as template DNA)	SLiCE
	JAZ2(R to K)_insert_Rv	GTACAGCGGCGCGGCGGCCTTCGTCTTCTTCTTCTCGAGGAAC		
pUGW45_eCFP-JAZ2-Jas$^{R\rightarrow K}$_vector	JAZ2_S.A.A._vector_Fw	GCCGCCGCGCCGCTGTAC	pUGW45_eCFP-JAZ2	SLiCE
	JAZ2(JAS R to K)_vector_Rv	TTTCTGCAGCGACTTCTTCATGGACAGCCCGCTCG		
pUGW45_eCFP-JAZ2-Jas$^{R, K\rightarrow A}$_insert	JAZ2(K,R to A)_insert_Fw	GCAGCATCGCTGCAGGCATTCCTCGAGGCAGCTGC	(primers used as template DNA)	SLiCE
	JAZ2(K,R to A)_insert_Rv	GTACAGCGGCGCGGCGGCTGCCGTTGCAGCTGCCTCGAGGAAT		
pUGW45_eCFP-JAZ2-Jas$^{R, K\rightarrow A}$_vector	JAZ2_S.A.A._vector_Fw	GCCGCCGCGCCGCTGTAC	pUGW45_eCFP-JAZ2	SLiCE
	JAZ2(JAS K,R to A)_vector_Rv	GCCTGCAGCGATGCTGCCATGGACAGCCCGCTCGC		
pUGW42_eYFP-TIFY-LCR2_insert	JAZ2_TIFY_SLiCE_Fw	AAAAAAGCAGGCTCCGCGAGGAGGAACTTGACCAT	pUGW45_eCFP-JAZ2	SLiCE
	JAZ2_LCR2_SLiCE_Rv	GCGCGCCCACCCTTCTACTGGTGGTAGTGGTGATC		
pUGW42_eYFP-LCR5-Jas_insert	JAZ2_LCR5_SLiCE_Fw2	AAAAAAGCAGGCTCCGCGGCGCTGGTTTCTCCTCG	pUGW45_eCFP-JAZ2	SLiCE
	JAZ2_JAS_SLiCE_Rv	GGCGCGCCCACCCTTCTA		
pUGW42_eYFP-TIFY-LCR2, pUGW42_eYFP-LCR5-Jas _vector	NLS-FLAG_SLiCE_Fw	TAGAAGGGTGGGCGCGCCGAC	pUGW45_eYFP-NLS-FLAG	SLiCE
	NLS-FLAG_SLiCE_Rv	CGCGGAGCCTGCTTTTTTGTACAAAC		
pGreenII-2x35S-TL-eCFP-JAZ2_insert	EGFP-F	CACCATGGTGAGCAAGGGCGAGGA	pUGW45_eCFP-JAZ2	SLiCE
	JAZ2-rv_SLiCE	CTC|TAGAGTCGCGGCCGCTCTATCGCCGGGCGTACAG		
pGreen II -2x35S-TL-eCFP-JAZ2_vector	pA35S-fw_SLiCE	AGCGGCCGCGACTCTAGAGTCC	pGreen II -2x35S-TL-eGFP	SLiCE
	EGFP-rv_SLiCE	TCCTCGCCCTTGCTCACCAT		
pGreen II -2x35S-TL-eCFP, pGreen II -2x35S-TL-eYFP_insert	EGFP-F	CACCATGGTGAGCAAGGGCGAGGA	pUGW45_eCFP-JAZ2, pUGW42_eYFP-JA:	SLiCE
	EGFP-R	TTACTTGTACAGCTCGTCCATG		
pGreen II -2x35S-TL-eCFP, pGreen II -2x35S-TL-eYFP_vector	EGFP-fw_SLiCE	GGACGAGCTGTACAAGTAA	pGreen II -2x35S-TL-eGFP	SLiCE
	EGFP-rv_SLiCE	TCCTCGCCCTTGCTCACCAT		
pGreen II -2x35S-TL-SCAMP1$^{\Delta N118}$-eYFP_insert	SCAMP1N119-fw_SLiCE	CGCGGCCGCGTCGACCATGCCTCCATTTCTGCCAC	pUGW42-SCAMP1$^{\Delta N118}$-eYFP	SLiCE
	EGFP-rv_SLiCE	TCCTCGCCCTTGCTCACCAT		
pGreen II -2x35S-TL-SCAMP1$^{\Delta N118}$-eYFP_vector	EGFP-F	CACCATGGTGAGCAAGGGCGAGGA	pGreen II -2x35S-TL-eGFP	SLiCE
	TEV-5'UTR-rv_SLiCE	GGTCGACGCGGCCGCGAAT		

Supplementary references

Cai Y, Jia T, Lam SK et al (2011) Multiple cytosolic and transmembrane determinants are required for the trafficking of SCAMP1 via an ER–Golgi–TGN–PM pathway. Plant J65:882-896. doi: 10.1111/j.1365-313X.2010.04469.x

Cai Y, Zhuang X, Wang J et al (2012) Vacuolar degradation of two integral plasma membrane proteins, AtLRR84A and OsSCAMP1, is cargo ubiquitination-independent and prevacuolar compartment-mediated in plant cells. Traffic 13:1023-1040. https://doi.org/10.1111/j.1600-0854.2012.01360.x